4 Theory of and Experimental Methods for the Acoustic Characterization of Wood

This chapter highlights the potential uses of vibrational methods in ultrasonic and audible frequency range for the characterization of mechanical behavior of solids in general and of wood-based composites in particular. The analysis of mechanical wave propagation in media of various complexities enables us to focus our attention on the theoretical basis of the techniques used for the measurement of elastic properties such as elastic moduli, Poisson's ratios, tensile or shear yield strengths, etc. The behavior of an acoustically vibrating body has been analyzed in fundamental reference books (Brillouin and Prodi 1956; Harris and Crede 1961; Hearmon 1961; Snowdon 1968; Truell et al. 1969; Musgrave 1970; Auld 1973; Achenbach 1973; Green 1973; Stephens and Levinthall 1974; Edmonds 1981; Rose 1999; Royer and Dieulesaint 2000).

The elastic properties of solids can be defined by the generalized Hooke's law relating the volume average of stress $[\sigma_{ij}]$ to the volume average of the strains $[\varepsilon_{kl}]$ by the elastic constants $[C_{ijkl}]$ in the form:

$$[\sigma_{ij}] = [C_{ijkl}] \cdot [\varepsilon_{kl}] \tag{4.1}$$

or

$$[\varepsilon_{kl}] = [S_{ijkl}] \cdot [\sigma_{ij}] \tag{4.2}$$

where $[C_{ijkl}]$ are termed elastic stiffnesses and $[S_{ijkl}]$ the elastic compliances, and i, j, k, or l correspond to 1, 2, 3, or 4. Stiffnesses and compliances are fourth-rank tensors. In his book, Hearmon (1961) noted that "the use of the symbols for compliances $[S]$ and $[C]$ for stiffness is now almost invariably followed." This is the notation that will be used hereafter.

$[C_{ijkl}]$ could be written, following the general convention on matrix notation, as $[C_{ij}]$, in terms of two-suffix stiffnesses, or symbolically as $[C]$. Similarly, $[S_{ijkl}]$ could be written as $[S_{ij}]$ or $[S]$. In many applications it is much simpler to write Eqs. (4.1) and (4.2) in the following condensed form:

$$[\sigma] = [C] \cdot [\varepsilon] \tag{4.2'}$$

and

$$[\varepsilon] = [S] \cdot [\sigma] \tag{4.2''}$$

It is apparent that the stiffness matrix $[C]$ is the inverse of the compliance matrix $[S]$, as $[C]=[S]^{-1}$ and $[S]=[C]^{-1}$.

Experimentally, the terms of the $[C_{ij}]$ matrix could be determined from ultrasonic measurements, whereas those of the $[S_{ij}]$ matrix could be determined from static tests.

From Eq. (4.1) it can be deduced that since strain is dimensionless the stiffnesses have the same dimensions as the stresses [the units used today are Newtons per square meter (N/m^2) or megapascals (MPa)]. As an example let us take the case of spruce in longitudinal direction, for which
$C_{11}=150\times10^8$ $N/m^2=15{,}000$ MPa=15 GPa.

For solids of different symmetries such as isotropic, transverse isotropic, or orthotropic, the stiffness matrix can be turned into a compliance matrix, following a specific procedure (Bodig and Jayne 1982). Symmetry features of solids are introduced by the material microstructural elements, i.e., orientation of the fibers.

4.1 Elastic Symmetry of Propagation Media

Because this chapter aims to provide the theoretical basis needed to understand wave propagation phenomena in solids, it was decided to analyze, first, the elastic symmetry of media of various complexity. For solid wood and for wood-based composites, orthotropic and transverse isotropic symmetries are most frequently observed. For simplicity, we will start by analyzing the isotropic solid. The solids are supposed to be homogeneous.

4.1.1 Isotropic Solids

The simplest elastic symmetry is that of an isotropic solid, with only two independent constants, λ and μ. The relationships between those constants are shown as follows:

$$\mu=\frac{E}{2(1+\nu)} \tag{4.3}$$

$$\lambda=\frac{E\cdot\nu}{(1+\nu)\cdot(1-2\nu)} \tag{4.4}$$

$$K=\frac{E}{3(1-2\nu)}=\lambda+\frac{2}{3}\mu \tag{4.5}$$

where E is Young's modulus (which is the ratio of longitudinal stress to longitudinal strain in the same direction of a rod), μ is the shear modulus (which is the ratio of the deviatoric stress to the deviatoric strain), V is the Poisson's ratio (the ratio of the transverse contraction of a sample to its longitudinal extension, under tensile stress), and K is the bulk modulus, with λ and μ the Lamé coefficients.

For an isotropic solid the stiffnesses are:

$$C_{11}=C_{22}=C_{33}=\lambda+2\mu \tag{4.6}$$

$$C_{12}=C_{23}=C_{13}=\lambda \tag{4.7}$$

$$C_{44}=C_{55}=C_{66}=\mu \tag{4.8}$$

The velocity of propagation of a bulk longitudinal wave in an infinite isotropic solid, initially assumed to be stress-free, is related to the elastic constants as:

$$V_L = \sqrt{\frac{E_{11}}{\rho}} = \sqrt{\frac{\lambda + 2\mu}{\rho}} \tag{4.9}$$

where ρ is the density, and λ and μ are the two Lamé constants.

The velocity of propagation of the transverse wave is related to the elastic constants by $V_T = \sqrt{\frac{\mu}{\rho}}$.

4.1.2 Anisotropic Solids

The origin of anisotropy, perceived as the variation in material response with direction of the applied stress, lies in the preferred organization of the internal structure of the material. The structure might be, for example, the atomic array in monocrystals, the morphological texture in polycrystalline aggregates such as metals, rocks, sand, etc., the orientation of fibers in composites and human tissue, or the orientation of layers in laminated plastics, plywood, etc.

One instance of complex elastic symmetry is that of an orthotropic solid, because constants are influenced by three mutually perpendicular planes of elastic symmetry. The corresponding stiffness matrix contains nine independent constants: six diagonal terms (C_{11}, C_{22}, C_{33}, C_{44}, C_{55}, C_{66}) and three off-diagonal terms (C_{12}, C_{13}, C_{23}), as can be seen from Eq. (4.11). For transverse isotropy, the material may possess an axis of symmetry in the sense that all directions at right angles to this axis are equivalent. The corresponding stiffness matrix (Eq. 4.12) contains five independent constants (C_{11}, C_{22}, C_{55}), four diagonal terms and two off-diagonal terms (C_{12}, C_{13}). It can be shown that the transverse isotropy is a particular case of an orthotropic solid.

The terms of the independent elastic constants are given below for the solids exhibiting different elastic symmetry.

Monoclinic material: 21 independent terms, and $C_{ij}=C_{ji}$:

$$\begin{bmatrix} C_{11} & C_{12} & C_{13} & C_{14} & C_{15} & C_{16} \\ C_{21} & C_{22} & C_{23} & C_{24} & C_{25} & C_{26} \\ C_{31} & C_{32} & C_{33} & C_{34} & C_{35} & C_{36} \\ C_{41} & C_{42} & C_{43} & C_{44} & C_{45} & C_{46} \\ C_{51} & C_{52} & C_{53} & C_{54} & C_{55} & C_{56} \\ C_{61} & C_{62} & C_{63} & C_{64} & C_{65} & C_{66} \end{bmatrix} \tag{4.10}$$

Orthotropic material: three symmetry axes, three symmetry planes, and nine independent terms of the stiffness matrix:

$$\begin{bmatrix} C_{11} & C_{12} & C_{13} & 0 & 0 & 0 \\ C_{21} & C_{22} & C_{23} & 0 & 0 & 0 \\ C_{31} & C_{32} & C_{33} & 0 & 0 & 0 \\ 0 & 0 & 0 & C_{44} & 0 & 0 \\ 0 & 0 & 0 & 0 & C_{55} & 0 \\ 0 & 0 & 0 & 0 & 0 & C_{66} \end{bmatrix} \tag{4.11}$$

Transverse isotropic material:

$$\begin{bmatrix} C_{11} & C_{12} & C_{13} & 0 & 0 & 0 \\ & C_{11} & C_{13} & 0 & 0 & 0 \\ & & C_{33} & 0 & 0 & 0 \\ & & & C_{44} & 0 & 0 \\ & & & & C_{44} & 0 \\ \text{symmetric} & & & & & (C_{11}-C_{12})/2 \end{bmatrix} \tag{4.12}$$

Isotropic material: two independent constants:

$$\begin{bmatrix} C_{11} & C_{12} & C_{12} & 0 & 0 & 0 \\ & C_{11} & C_{12} & 0 & 0 & 0 \\ & & C_{11} & 0 & 0 & 0 \\ & & & (C_{11}-C_{12})/2 & 0 & 0 \\ & & & & (C_{11}-C_{12})/2 & 0 \\ \text{symmetric} & & & & & (C_{11}-C_{12})/2 \end{bmatrix} \tag{4.13}$$

In summary, the number of constants for various types of anisotropic materials is 21 for monoclinic materials, 13 for triclinic materials, 9 for orthotropic materials, 5 for hexagonal or transversely isotropic materials, and 2 for isotropic materials.

The following is a brief discussion of the relationships between the engineering elastic parameters and the terms of stiffness and compliance matrices for solid wood, considered as an orthotropic material, and for composites of wood-based materials (plywood, flakeboards, fiberboards, etc.) expected to exhibit transverse isotropy. The discussion is based on the data presented in several fundamental references (Love 1944; Hearmon 1961; Green and Zerna 1968; Jayne 1972; Bodig and Jayne 1982; Guitard 1987).

First we consider the orthotropic symmetry of solid wood. The terms of the compliance matrix are given by Eq. (4.14):

$$\begin{bmatrix} S_{11} & S_{12} & S_{13} & 0 & 0 & 0 \\ S_{21} & S_{22} & S_{23} & 0 & 0 & 0 \\ S_{31} & S_{32} & S_{33} & 0 & 0 & 0 \\ & & & S_{44} & 0 & 0 \\ & & & & S_{55} & 0 \\ \text{symmetric} & & & & & S_{66} \end{bmatrix} \tag{4.14}$$

The physical significance of the compliances is as follows:

- S_{11} S_{22} S_{33} relate an extensional stress to an extensional strain, both in the same direction. For the particular symmetry of solid wood this relation gives the Young's moduli E_L, E_R, and E_T.
- S_{12} S_{13} S_{23} relate an extensional strain to a perpendicular extensional stress. In this way the six Poisson's ratios can be calculated.
- S_{44} S_{55} S_{66} relate a shear strain to a shear stress in the same plane,. and are the inverse of the terms C_{44} C_{55} C_{66}, corresponding to planes 23, 13, and 12.

The relationships between the stiffness terms and the compliance terms (Bodig and Jayne 1982) for the orthotropic solid are:

$$C_{11} = \frac{S_{22} \cdot S_{33} - (S_{23})^2}{S} \tag{4.15}$$

$$C_{22} = \frac{S_{11} \cdot S_{33} - (S_{13})^2}{S}$$

$$C_{33} = \frac{S_{22} \cdot S_{11} - (S_{12})^2}{S}$$

$$C_{12} = \frac{S_{21} \cdot S_{33} - S_{23} \cdot S_{31}}{S}$$

$$C_{13} = \frac{S_{31} \cdot S_{22} - S_{21} \cdot S_{32}}{S}$$

$$C_{23} = \frac{S_{31} \cdot S_{12} - S_{11} \cdot S_{32}}{S}$$

$$C_{44} = \frac{1}{S_{44}}; \; C_{55} = \frac{1}{S_{55}}; \; C_{66} = \frac{1}{S_{66}}$$

where

$$S = S_{11} \cdot S_{22} \cdot S_{33} + 2S_{12} \cdot S_{23} \cdot S_{31} - S_{11} \cdot {S_{23}}^2 - S_{22} \cdot {S_{13}}^2 - S_{33} \cdot {S_{12}}^2 \tag{4.16}$$

The terms of the compliance matrix are similarly related to the terms of the stiffness matrix, with the terms S replaced by the terms C.

When the axes are labeled 1, 2, 3 engineering constants are related to the compliances in the following way:

$$\begin{bmatrix} \frac{1}{E_1} & -\frac{\nu_{12}}{E_2} & -\frac{\nu_{13}}{E_3} & 0 & 0 & 0 \\ -\frac{\nu_{21}}{E_1} & \frac{1}{E_2} & -\frac{\nu_{23}}{E_3} & 0 & 0 & 0 \\ -\frac{\nu_{31}}{E_1} & -\frac{\nu_{32}}{E_2} & \frac{1}{E_1} & 0 & 0 & 0 \\ 0 & 0 & 0 & \frac{1}{G_{23}} & 0 & 0 \\ 0 & 0 & 0 & 0 & \frac{1}{G_{13}} & 0 \\ 0 & 0 & 0 & 0 & 0 & \frac{1}{G_{12}} \end{bmatrix} = [S] \tag{4.17}$$

Finally, it is worth recalling the relationships between the terms of stiffness matrix and the technical constants:

$$C_{11} = (1 - \nu_{23} \cdot \nu_{32}) \cdot [E_2 \cdot E_3 \cdot S]^{-1} \tag{4.18}$$

$$C_{22} = (1 - \nu_{13} \cdot \nu_{13}) \cdot [E_1 \cdot E_3 \cdot S]^{-1}$$

$$C_{33} = (1 - \nu_{13} \cdot \nu_{12}) \cdot [E_1 \cdot E_2 \cdot S]^{-1}$$

$$C_{12} = (\nu_{21} + \nu_{23} \cdot \nu_{31}) \cdot [E_2 \cdot E_3 \cdot S]^{-1}$$

$$C_{13} = (\nu_{13} + \nu_{12} \cdot \nu_{23}) \cdot [E_2 \cdot E_1 \cdot S]^{-1}$$

$$C_{23} = (\nu_{32} + \nu_{31} \cdot \nu_{12}) \cdot [E_1 \cdot E_3 \cdot S]^{-1}$$

$$C_{44} = G_{23}; C_{55} = G_{13}; C_{66} = G_{12}$$

and

$$S = [1 - \nu_{12} \cdot \nu_{21} - \nu_{23} \cdot \nu_{32} - \nu_{13} \cdot \nu_{31} - 2\nu_{21} \cdot \nu_{32} \cdot \nu_{31}] \cdot (E_1 \cdot E_2 \cdot E_3)^{-1} \tag{4.18'}$$

Accurate measurement of the set of orthotropic constants is not an easy task. Among these constants, Poisson's ratios ν_{ij} are perhaps the most difficult to measure. For a more thorough understanding of the problem, the realistic boundaries of Poisson's ratios have also to be considered. The reasons that underlie this observation are described below, first by analyzing the isotropic solids and second by analyzing the orthotropic solids.

For an isotropic solid, the relationships (Green and Zerna 1968) between the Poisson's ratios (defined as the quotient "lateral constriction/longitudinal extension") for a specimen under tension and the elastic constants are:

– for the bulk modulus K

$$-1 < \nu < ½ \tag{4.19}$$

– for the shear modulus

$$G = \frac{E}{2}(1 + \nu) \tag{4.20}$$

where ν is the Poisson's ratio, E is the Young's modulus, and G is the shear modulus, also called the Coulomb modulus.

The strain energy function is positive definite for an homogeneous isotropic elastic continuum. This means that $K>0$ and $G>0$. Consequently $E>0$ and $(1–2\nu)>0$ or $(1–\nu)>0$. The boundary conditions for Poisson's ratios are:

$$-1 < \nu < ½ \tag{4.21}$$

For an orthotropic solid, the question is more complex due to the six Poisson's ratios, corresponding to the three symmetry planes. Bearing in mind that the strain energy function W must be defined as positive, we form:

$$W=\frac{1}{2}\cdot C_{\mathrm{ijkl}}\cdot\varepsilon_{\mathrm{ij}}\cdot\varepsilon_{\mathrm{kl}}\cdot>0 \tag{4.22}$$

and similarly

$$W=\frac{1}{2}\cdot S_{\mathrm{ijkl}}\cdot\sigma_{\mathrm{ij}}\cdot\sigma_{\mathrm{kl}}\cdot>0 \tag{4.23}$$

Consequently, $C_{ijkl}>0$ and $S_{ijkl}>0$, meaning that all the terms of the stiffness and compliance matrices must be positive, or in other words:

$$C_{11},\ C_{22},\ C_{33},\ C_{44},\ C_{55},\ C_{66},\ C_{12},\ C_{13},\ C_{23}>0 \tag{4.24}$$

$$S_{11},\ S_{22},\ S_{33},\ S_{44},\ S_{55},\ S_{66},\ S_{12},\ S_{13},\ S_{23}>0 \tag{4.24'}$$

For a real material, the Young's moduli and the shear moduli must also be positive definite as:

$$E_1,\ E_2,\ E_3,\ G_{12},\ G_{13},\ G_{23}>0 \tag{4.25}$$

Considering now the relationships between the terms of the [C] and [S] matrices and the engineering constants, we can deduce the boundary conditions for all Poisson's ratios of an orthotropic solid. From Equation (4.18) we can establish the simultaneous relationships between all six Poisson's numbers:

$$[1-\nu_{12}\cdot\nu_{21}-\nu_{23}\cdot\nu_{32}-\nu_{13}\cdot\nu_{31}-2\nu_{21}\cdot\nu_{32}\cdot\nu_{31}]>0 \tag{4.26}$$

The relationships between two Poisson's ratios, corresponding to a well-defined symmetry plane, are deduced from Eq. (4.18) when the terms C_{11}, C_{22}, and C_{33} are considered as

$$1-\nu_{12}\cdot\nu_{21}>0;1-\nu_{13}\cdot\nu_{31}>0;1-\nu_{32}\cdot\nu_{23}>0; \tag{4.27}$$

From these equation we recognize that the corresponding in-plane Poisson's ratios ν_{rq} and ν_{qr} could both have the same sign (+) or (−). On the other hand, the relationship between Poisson's ratios and Young's moduli is $-\nu_{rq}/\mathrm{E_r}=-\nu_{qr}\times/\mathrm{E_q}$, and

$$\nu_{\mathrm{rq}}=\nu_{\mathrm{rq}}\cdot\mathrm{E_q}/\mathrm{E_r} \tag{4.28}$$

However, for anisotropic solids it is possible to have $\mathrm{E_r}>\mathrm{E_q}$ and therefore $\nu_{qr}>1$.

Table 4.1A. Engineering parameters of solid wood: Young's moduli and shear moduli. (Hearmon 1948)

Species	Density (kg/m^3)	Young's moduli ($10^8 N/m^2$)			Shear moduli ($10^8 N/m^2$)		
		$E_{1=}E_L$	$E_{2=}E_R$	$E_{3=}E_T$	$G_{44=}G_{RT}$	$G_{55=}G_{LT}$	$G_{66=}G_{LR}$
Balsa	200	6.3	3.0	1.1	0.3	2.0	3.1
Yellow polar	380	97	8.9	4.1	1.1	6.7	7.2
Birch	620	163	11.1	6.2	1.9	9.2	11.8
Oak	660	53	21.4	9.7	3.9	7.6	12.9
Ash	670	158	15.1	8.0	2.7	8.9	13.4
Beech	750	137	22.4	11.4	4.6	10.6	16.1
Sitka spruce	390	116	9.0	5.0	0.39	7.2	7.5
Spruce	440	159	6.9	3.9	0.36	7.7	7.5
Douglas fir	450	157	10.6	7.8	0.88	8.8	8.8
Fir	450	127	9.3	4.8	1.40	7.5	9.3
Scotch pine	550	163	11.0	5.7	0.66	6.8	11.6

Table 4.1B. Engineering parameters of solid wood: Poisson's ratios. (Hearmon 1948)

Species	Density (kg/m^3)	Poisson's ratios					
		$\nu_{12=}\nu_{LR}$	$\nu_{21=}\nu_{RL}$	$\nu_{13=}\nu_{LT}$	$\nu_{31=}\nu_{TL}$	$\nu_{23=}\nu_{RT}$	$\nu_{32=}\nu_{TR}$
Balsa	200	0.23	0.018	0.49	0.009	0.66	0.24
Yellow polar	380	0.32	0.030	0.39	0.019	0.70	0.33
Birch	620	0.49	0.034	0.43	0.018	0.78	0.38
Oak	660	0.33	0.130	0.50	0.086	0.64	0.30
Ash	670	0.46	0.051	0.51	0.030	0.71	0.36
Beech	750	0.45	0.073	0.51	0.044	0.75	0.36
Sitka spruce	390	0.37	0.029	0.47	0.020	0.43	0.25
Spruce	440	0.44	0.028	0.38	0.013	0.47	0.25
Douglas fir	450	0.29	0.020	0.45	0.022	0.39	0.37
Fir	450	0.45	0.030	0.50	0.020	0.60	0.35
Scotch pine	550	0.42	0.038	0.51	0.015	0.68	0.31

Indeed, negative values of Poisson's ratios or values greater than 1 may contradict our intuition if our main experience is dealing with isotropic solids, but such data have been reported for composite materials (Jones 1975) and for foam material (Lipsett and Beltzer 1988), cellular materials (Gibson and Ashby 1988), crystals, wood (McIntyre and Woodhouse 1986), and wood-based composites (Bucur and Kazemi-Najafi 2002).

In their excellent review of methods used to measure mechanical properties, McIntyre and Woodhouse (1986) suggested that idealized two-dimensional honeycomb patterns of transverse wood structure could produce a Poisson's ratio ν_{RT} in the range: -1 to $+\infty$.

Referring to the analysis above, the assumption of orthotropy suggests that nine independent stiffnesses or compliances characterize the elastic behavior of solid wood analyzed in a rectangular coordinate system. As a consequence, we find 12

Table 4.2. Elastic constants ($\times 10^8$ N/m^2) of three ply "equivalent material" of birch and sitka spruce compared with those of solid wood. (Gerhards 1987, with permission)

Specimens	Dynamic moduli (10^8N/m^2)					
	E_1	E_2	E_3	G_{44}	G_{55}	G_{66}
Birch three plywood	96.6	54.1	27.0	6.04	8.78	10.6
	95.1	53.3	22.4	6.04	8.78	10.6
Sitka spruce three plywood	79.6	42.3	9.9	0.57	10.6	7.2
	79.0	42.0	9.0	0.57	10.6	7.2
Birch solid wood	163	11	6.2	1.9	11.8	9.1
Sitka spruce solid wood	116	9.0	5.0	0.4	7.5	7.2

Table 4.3. Elastic constants of machine-made heavy bleached kraft milk carton stock. (Data from Baum et al. 1981)

Young's moduli (10^8N/m^2)			Shear moduli (10^8N/m^2)		
E_1	E_2	E_3	G_{44}	G_{55}	G_{66}
74.4	34.7	0.39	0.99	1.37	20.4
Poisson's ratios					
ν_{12}	ν_{21}	ν_{13}	ν_{31}	ν_{23}	ν_{32}
0.15	0.32	0.008	1.52	0.021	1.84

engineering parameters: three Young's moduli, three shear moduli, and six Poisson's ratios. Table 4.1 gives some values of solid wood engineering parameters.

For a very wide range of European, American, and tropical species, Bodig and Goodmann (1973) as well as Guitard (1987) and Guitard and Geneveaux (1988) deduced statistical regression models able to predict the terms of the compliance matrix as a function of density. These data may be used by modelers in finite element calculations, or with nondestructively tested lumber when the elasticity moduli are required. In engineering practice, however, the elastic constants of solid wood could be used for accurate estimation of the elastic properties of plywood. Gerhards (1987) defined a homogeneous "equivalent orthotropic material" that enables conventional analysis methods to be applied for elastic characterization of plywood. Gerhard's approach is deduced from the "strain energy" method. The properties of the proposed material are compared with those of an equivalent material deduced from the "law of mixtures" proposed previously by Bodig and Jayne (1982). The values of Young's moduli and shear moduli for the "equivalent plywood" and for solid wood are given in Table 4.2. Plywood exhibits less anisotropic mechanical properties than solid wood. Young's moduli E_2 and E_3 as well as shear modulus G_{23} for plywood are strongly increased compared to the same properties of solid wood.

Another interesting example of an orthotropic wood composite is that of machine-made paper. Mann et al. (1980) describe the measurement of nine elastic constants using a transmission technique on a heavy milk carton stock (780 kg/m^3). The engineering constants are presented in Table 4.3. These constants indicate that

the paperboard is highly anisotropic. The Poisson's ratios corresponding to the planes that include axis 3, the axis normal to the thickness, are remarkably high, undoubtedly tied-up with the misalignment of fibers in the plane of the sheet.

For wood composites exhibiting plane isotropy, also called transverse anisotropy (seven constants), or for some tropical wood species, the terms of the stiffness matrix can be reduced, bearing in mind that:

$$C_{11} = C_{22;\text{ and}}\, C_{66} = \frac{C_{11} - C_{12}}{2} \tag{4.29}$$

For this solid having transverse anisotropy (Vinh 1982), the corresponding relationships between the terms of the stiffness matrix and the engineering constants are:

$$E_1 = \frac{\left(C_{11} - \frac{C_{13}^2}{C_{33}}\right)^2 - \left(C_{12} - \frac{C_{13}^2}{C_{33}}\right)^2}{C_{11} - \frac{C_{13}^2}{C_{33}}} \tag{4.30}$$

$$E_3 = C_{33} - 2C_{13}^2 / (C_{11} + C_{12})$$

$$\nu_{12} = \nu_{21} = \frac{C_{12} \cdot C_{33} - C_{13}^2}{C_{11} \cdot C_{33} - C_{13}^2}$$

$$\nu_{13} = \frac{C_{13} \cdot (C_{11} - C_{12})}{C_{11} \cdot C_{33} - C_{13}^2}$$

$$\nu_{31} = \frac{C_{13}}{C_{11} + C_{12}}$$

$$C_{55} = G_{13}$$

$$C_{66} = G_{12}$$

The corresponding relationships between the terms of the compliance matrix and the engineering terms are given by Eq. (4.31), if $E_1=E_2=E$; $\nu_{12}=\nu_{21}=\nu$; $G_{12}=G+E/2(1+\nu)$:

$$\begin{bmatrix} \frac{1}{E} & -\frac{\nu}{E} & -\frac{\nu_{31}}{E_3} & 0 & 0 & 0 \\ -\frac{\nu}{E} & \frac{1}{E} & -\frac{\nu_{32}}{E_3} & 0 & 0 & 0 \\ -\frac{\nu_{13}}{E} & -\frac{\nu_{23}}{E} & \frac{1}{E_3} & 0 & 0 & 0 \\ 0 & 0 & 0 & \frac{1}{G_{23}} & 0 & 0 \\ 0 & 0 & 0 & 0 & \frac{1}{G_{13}} & 0 \\ 0 & 0 & 0 & 0 & 0 & \frac{E}{2(1+\nu)} \end{bmatrix} = [S] \tag{4.31}$$

Note that seven is the total number of independent stiffnesses or compliances derived from the particular form of Hooke's law for plane isotropic solids. Correspondingly, the number of engineering elastic parameters is nine, i.e., two Young's moduli, two shear moduli, and five Poisson's ratios. Using transverse isotropic hypothesis for the structure of a standing tree, Archer (1986) presented a procedure for growth strain estimation. The same symmetry was used by Baum and Bornhoeft (1979) for the estimation of Poisson's ratios in paper.

4.2 Wave Propagation in Anisotropic Media

The propagation of waves in isotropic and anisotropic solids has been discussed in many reference books (Angot 1952; Hearmon 1961; Fedorov 1968; Musgrave 1970; Auld 1973; Green 1973; Dieulesaint and Royer 1974; Alippi and Mayer 1987; Rose 1999).

Let us consider first the case of an isotropic solid in which bulk waves are propagating. When the particle motion is along the propagation direction, we have a longitudinal wave. When the particle motion is perpendicular to the propagation direction, we have a shear wave or a transverse wave. In anisotropic materials both longitudinal and transverse waves can propagate either along the principal symmetry directions or out of them. Figure 4.1 shows the case of an orthotropic solid. Surface waves can propagate in any direction on any isotropic or anisotropic substrate, and can be used for the characterization of elastically anisotropic solids having piezoelectric properties as well as the characterization of layered solids (Edmonds 1981).

In this section some theoretical considerations will be presented in relation to the propagation phenomena of ultrasonic waves in orthotropic solids. This symmetry was chosen because of the interest in the Cartesian orthotropic wood structure model. As can be seen in this chapter, the most rapid way to obtain stiffnesses is by the ultrasonic velocity method.

The notations used in this chapter are as follows:

$[\sigma]$ =stress tensor
$[\varepsilon]$ =strain tensor
ρ =density
$[C_{ijkl}]$ =stiffness tensor
$[S_{ijkl}]$ =compliance tensor
$[\Gamma_{ij}]$ =Christoffel tensor
$\mathbf{u}$ =displacement vector
$\mathbf{n}$ =propagation vector
U_i =components of the amplitude of the displacement vector
P =polarization vector
P_m =components of the unit vector in the direction of the displacement or polarization
k_m =wave vector component along the x_m direction
k =wave vector
x_m =position vector
ω =angular frequency
n_k =direction cosines
α =angle of unit wave vector from symmetry direction
β =displacement angle
δ_{ik} =Kronecker tensor; if $i=k$ then $\delta_{ik}=1$ and if $i\neq k$, $\delta_{ik}=0$

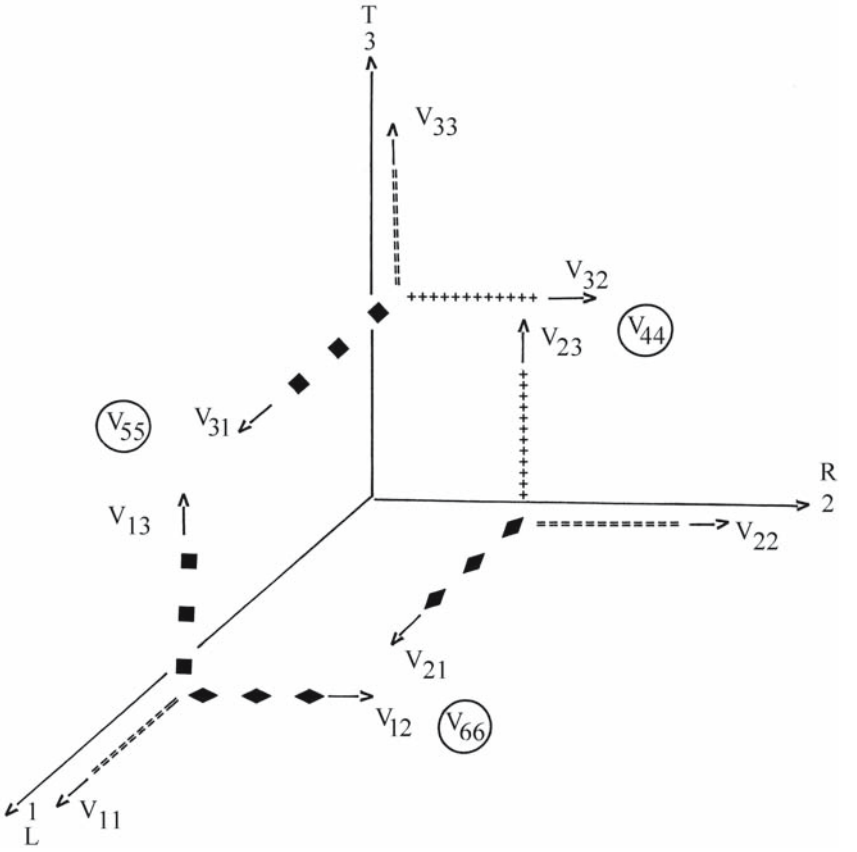

Fig. 4.1. Ultrasonic velocities in an orthotropic solid. $V_{11}=V_{LL}$, $V_{22}=V_{RR}$, $V_{33}=V_{TT}$, $V_{44}=V_{RT}$, $V_{55}=V_{LT}$, $V_{66}=V_{LR}$

D_{ij} =flexural rigidities in plates
ν_{ij} =Poisson's ratios
t =time
v_{phase} =V=phase velocity
v =group velocity
$a_1 \ldots a_4$ =coefficients depending on the supported conditions of a plate
A =amplitude

4.2.1 Propagation of Ultrasonic Bulk Waves in Orthotropic Media

The generalized Hook's law can be written as we have seen previously (Eq. 4.1):

$$\sigma_{ij} = C_{ijkl} \cdot \varepsilon_{kl} \tag{4.32}$$

or in the form $[\sigma]=[C][\varepsilon]$, where $[\sigma_{ij}]$ is the stress tensor and the stress is in direction $_i$ acting on the surface, with its normal in the direction j. The elasticity tensor

$[C_{ijkl}]$, also written as $[C]$, is a fourth-order tensor with 81 components which describes the proportionality between the stress tensor and strain or deformation tensor, which are both second-rank tensors.

The strain tensor $[\varepsilon_{kl}]$ of small deformation of the material under stress related linearly to the displacement u as:

$$\varepsilon_{kl} = \frac{1}{2}\left(\frac{\partial u_k}{\partial x_l} + \frac{\partial u_l}{\partial x_k}\right) \tag{4.33}$$

The symmetry of the stress and strain tensors imposes the following restrictions on the stiffness tensor $[C]$: $C_{ijkl}=C_{jikl}=C_{ijlk}=C_{jilk}$. It also reduces the number of independent components from 81 to 21.

The elastodynamic equations for a continuum with no forces acting on it are:

$$\frac{\partial \sigma_{ij}}{\partial x_j} = \rho \frac{\partial^2 u_i}{\partial t^2} \tag{4.34}$$

By combining the before mentioned equations, the equation of wave can be written as:

$$\rho \frac{\partial^2 u_i}{\partial t^2} - C_{ijkl} \frac{\partial^2 u_k}{\partial x_l \cdot \partial x_j} = 0 \tag{4.35}$$

If we assume a plane harmonic wave with the displacement u propagating in the direction of the unit vector n, normal to the wavefront, we have:

$$u_i = A_i \cdot \exp\{i(k_j \cdot x_j - \omega t)\} \tag{4.36}$$

The unit wave vector k_j can be written as $\mathrm{k} = \frac{2\pi}{\lambda}\mathrm{n} = \frac{\omega}{\mathrm{v}_{phase}}\mathrm{n}$.

For the amplitude we can write $A_i = AP_m$ where P_m are the components of the unit vector in the direction of displacement (polarization). After substitution, the equation of motion takes the form:

$$(\mathrm{C}_{ijkl}\,\mathrm{n}_j\,\mathrm{n}_k - \delta_{ik}\,\rho\,\mathrm{v}^2_{\mathrm{phase}})\,\mathrm{P}_\mathrm{m} = 0 \tag{4.37}$$

By introducing the Kelvin-Christoffel tensor, Γ, we can write

$$\Gamma_{ik} = \mathrm{C}_{ijkl}\,\mathrm{n}_j\,\mathrm{n}_l$$

and

$$(\Gamma_{ik} - \delta_{ik}\,\rho\,\mathrm{v}^2_{\mathrm{phase}})\,\mathrm{P}_\mathrm{m} = 0 \tag{4.38}$$

These are the Christoffel's equations valid for the most general kind of anisotropic solids.

Christoffel's equations supply the relations between the elastic constants C_{ijkl} and the phase velocity v_{phase}=V of ultrasonic waves propagating in the medium.

The coefficients of the tensor

$$\Gamma_{ik=}\begin{vmatrix} \Gamma_{11} & \Gamma_{12} & \Gamma_{13} \\ \Gamma_{21} & \Gamma_{22} & \Gamma_{23} \\ \Gamma_{31} & \Gamma_{32} & \Gamma_{33} \end{vmatrix}$$

are given in the following table, for the general case of stiffness tensor with 21 terms (Dieulesaint and Royer 1974), for which $\Gamma_{12}=\Gamma_{21}$, $\Gamma_{13}=\Gamma_{31}$, and $\Gamma_{23}=\Gamma_{32}$:

Γ_{ij}	Terms of stiffness tensor			
	Terms with $n_1^2n_2^2n_3^2$	Terms with $2n_2n_3$	Terms with $2n_1n_3$	Terms with $2n_1n_2$
Γ_{11}	$n_1^2C_{11}$, $n_2^2C_{66}$, $n_3^2C_{55}$	C_{56}	C_{15}	C_{16}
Γ_{22}	$n_1^2C_{66}$, $n_2^2C_{22}$, $n_3^2C_{44}$	C_{24}	C_{46}	C_{26}
Γ_{33}	$n_1^2C_{55}$, $n_2^2C_{44}$, $n_3^2C_{33}$	C_{34}	C_{35}	C_{45}
Γ_{12}	$n_1^2C_{16}$, $n_2^2C_{26}$, $n_3^2C_{45}$	$1/2(C_{25}+C_{46})$	$1/2(C_{14}+C_{56})$	$1/2(C_{12}+C_{66})$
Γ_{13}	$n_1^2C_{15}$, $n_2^2C_{46}$, $n_3^2C_{35}$	$1/2(C_{36}+C_{45})$	$1/2(C_{13}+C_{55})$	$1/2(C_{14}+C_{56})$
Γ_{23}	$n_1^2C_{56}$, $n_2^2C_{24}$, $n_3^2C_{34}$	$1/2(C_{23}+C_{44})$	$1/2(C_{36}+C_{45})$	$1/2(C_{25}+C_{46})$

Example: in the general case we have for $\Gamma_{11}=n_1^2C_{11}+n_2^2C_{66}+n_3^2C_{55}+2n_2n_3C_{56}+2n_1n_3C_{15}+2n_1n_2C_{16}$.

For an orthotropic solid, with nine terms of stiffness tensor [C] and three elastic symmetry planes we have:

- in symmetry plane 12: $n_1=\cos\alpha$; $n_2=\sin\alpha$; $n_3=0$ and the stiffnesses C_{11}; C_{22}; C_{66}; $\Gamma_{11}=C_{11}n_1^2+C_{66}n_2^2$; $\Gamma_{22}=C_{22}n_2^2+C_{66}n_1^2$; $\Gamma_{12}=(C_{12}+C_{66})n_1n_2$;
- in symmetry plane 13: $n_1=\cos\alpha$; $n_3=\sin\alpha$; $n_2=0$ and the stiffnesses C_{11}; C_{33}; C_{55};$\Gamma_{11}=C_{11}n_1^2+C_{55}n_3^2$; $\Gamma_{33}=C_{33}n_3^2+C_{55}n_1^2$; $\Gamma_{23}=(C_{13}+C_{55})n_1n_3$;
- in symmetry plane 23: $n_2=\cos\alpha$; $n_3=\sin\alpha$; $n_1=0$ and the stiffnesses C_{22}; C_{33}; C_{44}; $\Gamma_{22}=C_{22}n_2^2+C_{44}n_3^2$; $\Gamma_{33}=C_{33}n_3^2+C_{44}n_2^2$; $\Gamma_{23}=(C_{23}+C_{44})n_2n_3$;

4.2.1.1 Velocities and Stiffnesses, the Eigenvalues of Christoffel's Equations

The eigenvalues and the eigenvectors of Christoffel's equations can be calculated for specific anisotropic materials. The nonzero values of the displacements – polarization – are obtained as characteristic eigenvectors corresponding with the characteristic eigenvalues which are the roots of Eq. (4.37).

$$\begin{bmatrix} \Gamma_{11}-\rho\cdot V^2 & \Gamma_{12} & \Gamma_{13} \\ \Gamma_{21} & \Gamma_{22}-\rho\cdot V^2 & \Gamma_{23} \\ \Gamma_{31} & \Gamma_{32} & \Gamma_{33}-\rho\cdot V^2 \end{bmatrix}\begin{bmatrix} p_1 \\ p_2 \\ p_3 \end{bmatrix}=0 \tag{4.40}$$

This equation is a cubic polynomial in phase velocity squared. From it the first issue addressed is the determination of the elastic constants (Γ_{ij}) of a given material, when the phase velocity is known. This equation forms a set of simultaneous equations in p_m (p_1, p_2, p_3), or for a unique solution to those we have to fulfill the condition of Eq. (4.41):

$$\begin{bmatrix} \Gamma_{11}-\rho\cdot V^2 & \Gamma_{12} & \Gamma_{13} \\ \Gamma_{21} & \Gamma_{22}-\rho\cdot V^2 & \Gamma_{23} \\ \Gamma_{31} & \Gamma_{32} & \Gamma_{33}-\rho\cdot V^2 \end{bmatrix} = 0 \tag{4.41}$$

If this equation is written for wave propagation along the symmetry axes for an orthotropic solid, we obtain three solutions:

$$\begin{bmatrix} \Gamma_{11}-\rho\cdot V^2 & 0 & 0 \\ 0 & \Gamma_{22}-\rho\cdot V^2 & 0 \\ 0 & 0 & \Gamma_{33}-\rho\cdot V^2 \end{bmatrix} = 0 \tag{4.42}$$

These solutions show that along every axis it is possible to have three types of waves, i.e., one longitudinal and two transverse, as can be seen from the following equations (Eq. 4.43):

$$\begin{aligned} &\Gamma_{11}-\rho\cdot V^2 =; \rho\cdot V^2 = C_{11}, \text{ corresponding to a longitudinal wave} \\ &\Gamma_{22}-\rho\cdot V^2 = 0; \rho\cdot V^2 = C_{66}, \text{ corresponding to a fast shear wave} \\ &\Gamma_{33}-\rho\cdot V^2 = 0; \rho\cdot V^2 = C_{55}, \text{ corresponding to a slow shear wave} \end{aligned} \tag{4.43}$$

Such solutions enable us to calculate the six diagonal terms of stiffness matrix [C] by a relation which may be presented in the following general form:

$$C_{ii}-\rho\cdot V^2 \text{ where i = 1, 2, 3, ...6} \tag{4.44}$$

The three off-diagonal stiffness components can be calculated when the propagation is out of the principal axes of symmetry of the solid as, for example, in plane 12:

$$\begin{bmatrix} \Gamma_{11}-\rho\cdot V^2 & \Gamma_{12} & 0 \\ \Gamma_{21} & \Gamma_{22}-\rho\cdot V^2 & 0 \\ 0 & 0 & \Gamma_{33}-\rho\cdot V^2 \end{bmatrix} = 0 \tag{4.45}$$

or in other words,

$$(C_{12}+C_{66})n_1n_2 = \pm\left[(C_{11}n^2{}_1 + C_{66}n^2{}_2 - \rho\cdot V_\alpha{}^2)\,(C_{66}n^2{}_1 + C_{22}n^2{}_2 - \rho\cdot V_\alpha{}^2)\right]^{1/2} \tag{4.46}$$

where V_α depends on the angle of propagation α, out of the principal direction of quasi-longitudinal or quasi-shear bulk waves, in infinite solids.

By permutations of indices we obtain the corresponding expression for C_{13} and C_{23}. Details of the calculation are given in Table 4.4.

If we admit that the matrix [C] >0 and consequently C_{ij} >0, then for the propagation angle α, considered as $0<\alpha<\pi/2$ or $\pi<\alpha<3\pi/2$, the expression under square root (Eq. 4.46) must be considered with the sign (+). For other angles the expression under the square root must be taken with the sign (−)

Table 4.4. Propagation of bulk waves in an orthotropic solid. *L* Longitudinal wave; *T* transverse wave; *QL* quasi-longitudinal wave ; *QT* quasi-transverse wave; bold indicates that for ±, one takes + for the calculation of the QL wave velocity and − for the calculation of the QT wave velocity

Propagation direction	Wave Normal	Polarization vector	Wave Type	Velocity and stiffnesses
Propagation along principal directions of elastic symmetry				
Axis X_1	$\boldsymbol{n_1=1}$	X_1	L	$\boldsymbol{V_{11}^2\times\rho=C_{11}}$
	$n_2=0$	X_2	T	$V_{66}^2\times\rho=C_{66}$
	$n_3=0$	X_3	T	$V_{55}^2\times\rho=C_{55}$
Axis X_2	$n_1=0$	X_1	T	$V_{66}^2\times\rho=C_{66}$
	$\boldsymbol{n_2=1}$	X_2	L	$\boldsymbol{V_{22}^2\times\rho=C_{22}}$
	$n_3=0$	X_3	T	$V_{44}^2\times\rho=C_{44}$
Axis X_3	$n_1=0$	X_1	T	$V_{55}^2\times\rho=C_{55}$
	$n_2=0$	X_2	T	$V_{44}^2\times\rho=C_{44}$
	$\boldsymbol{n_3=1}$	X_3	L	$\boldsymbol{V_{33}^2\times\rho=C_{33}}$
Propagation out of principal directions				
Plane: X_1 X_2	n_1, n_2	$p_1/p_2=\Gamma_{12}/(\rho V^2-\Gamma_{11})=(\rho V^2-\Gamma_{22})/\Gamma_{12}$	QL, QT	$2\rho V^2_{QL,\,QT}=(\Gamma_{11}+\Gamma_{22})\pm[(\Gamma_{11}-\Gamma_{22})^2+4\Gamma_{12}^2]^{1/2}$
	$n_3=0$	X_3	T	$\rho V_T^{2=}C_{55}\,n_1^2+C_{44}\,n_2^2$
Plane: X_1 X_3	n_1, n_3	$p_1/p_3=\Gamma_{13}/(\rho V^2-\Gamma_{11})=(\rho V^2-\Gamma_{33})/\Gamma_{13}$	QL, QT	$2\rho V^2_{QL,\,QT}=(\Gamma_{11}+\Gamma_{33})\pm[(\Gamma_{11}-\Gamma_{33})^2+4\Gamma_{13}^2]^{1/2}$
	$n_2=0$	X_2	T	$\rho V_T^{2=}C_{66}\,n_1^2+C_{44}\,n_2^2$
Plane: X_2 X_3	n_2, n_3	$p_1/p_3=\Gamma_{23}/(\rho V^2-\Gamma_{22})=(\rho V^2-\Gamma_{33})/\Gamma_{13}$	QL, QT	$2\rho V^2_{QL,\,QT}=(\Gamma_{22}+\Gamma_{33})\pm[(\Gamma_{22}-\Gamma_{33})^2+4\Gamma_{23}^2]^{1/2}$
	$n_1=0$	X_1	T	$\rho V_T^{2=}C_{55}\,n_1^2+C_{66}\,n_2^2$

In the interests of clarity, for the calculation of the off-diagonal terms of the stiffness matrix C_{12}, C_{13}, and C_{23} we insist on having the value of the velocity of a quasi-longitudinal or quasi-shear wave, or both of them. It should also be noted that those values are dependent on the propagation vector and consequently on the orientation of the specimen (angle α).

It is well known that the physical properties of wood are strongly dependent on the orientation of reference coordinates or, in other words, they are dependent on the angle α mentioned before. This directional dependency of wood constants renders conventional averaging techniques inapplicable when measurements are taken with specimens at different angles. For this reason Chapter 5 provides rational procedures for data averaging (or optimization) of directionally dependent measurements.

Having now obtained optimized values for all nine terms of the stiffness matrix [*C*], the calculation of engineering constants − Young's moduli and Poisson's ratios − can easily be carried out (Eq. 4.18). The matrix [*C*] is inverted to obtain the compliance terms of [*S*], and subsequently Young's moduli and Poisson's ratios are determined using simple relations, as we have seen previously (Eq. 4.17).

The values of the [*C*] matrix, when an optimization procedure for off-diagonal terms was used (see Chap. 5), could be employed for the calculation of the characteristic velocity surfaces or its inverse, slowness ($^1/_V$) surfaces. The velocity surface is the locus of the radius vector, which has a length proportional to the velocity in the direction of the vector. The slowness surface is formed with the

radius proportional to $(^1/_V)$. The normal to the slowness surface coincides with the direction of the flux energy. The wave surface is the polar reciprocal of the slowness surface. For isotropic materials both the slowness surface and the wave surface are spheres.

The velocity surface is known to be formed by the intersection of three separate surfaces (sheets) (Musgrave 1970). These are named quasi-longitudinal (QL), quasi-transverse (also called quasi-shear and fast shear wave) (QT), and transverse (also called slow shear wave) (T), and they are calculated using the corresponding velocities.

As an example let us consider them in plane 12 of an orthotropic solid, with the following equations (Eq. 4.47):

$$2\rho V^2{}_{QL} = (\Gamma_{11}+\Gamma_{22}) + [(\Gamma_{11}-\Gamma_{22})^2 + 4\Gamma^2{}_{12}]^{1/2} \text{ (corresponding to QL wave)} \quad (4.47)$$

$$2\rho V^2{}_{QT} = (\Gamma_{11}+\Gamma_{22}) - [(\Gamma_{11}-\Gamma_{22})^2 + 4\Gamma^2{}_{12}]^{1/2} \text{ (corresponding to QL wave = fast shear wave)}$$

$$\rho V_T{}^2 = C_{55}n_1{}^2 + C_{44}n_2{}^2 \text{ (T wave = slow shear wave, with polarization in axis 3)}$$

Figure 4.2 shows the velocity surface of an orthotropic solid (beech). These curves help to establish the discrepancies between the theoretical and experimental values of velocities and to quantify the anisotropy of materials.

Musgrave (1970) demonstrated that wave propagation in any medium can be represented by the velocity surface, the slowness surface (the inverse of velocity), and the wave surface. Figure 4.3 shows, for historic interest, the slowness surface and wave surface of solids with orthorhombic symmetry (uranium and spruce). Several intersection points can be observed on the slowness surface between sheets, demonstrating the mode conversion phenomena. To identify the displacement vectors, the conditions of cusps must be studied on the wave surface. The cusps are associated with the departure of the slowness surface from an elliptical shape.

Moreover, the flux energy in anisotropic media deviates from the wave normal. Figure 4.4 gives an example of energy flux deviation in transversely isotropic graphite fibers (Kriz and Stinchcomb 1979). The deviation of energy flux from the wave normal can generate phenomena of conical refraction of waves.

Ultrasonic energy propagation through wood was studied by Berndt et al. (2000) and Bucur and Berndt (2001). In wood, as in other anisotropic materials, the group velocity vector generally differs from the phase velocity vector. The group velocity vector is normal to the slowness surface of a wave mode (Musgrave 1970; Auld 1973). While the propagation vectors of the three modes (QL, QT, and T) are identical (at the angle α), the energy flux vectors depend on the mode. The angle of energy flux deviation can be calculated and verified experimentally, by holding the sending transducer stationary while scanning with the receiving transducer for the maximum energy for each mode, keeping the transducer axes parallel. The angle of flux deviation can be calculated from the lateral beam offset and the sample thickness, using simple trigonometry (Berndt et al. 2000). Figure 4.5 shows the flux deviation in QL and QT modes in the LT plane for oak and Douglas fir. The choice is very illustrative because of the high anisotropy in elastic properties between the L and T directions. Wave behavior in this plane is also important in the application of ultrasonics in wood evaluation, because this

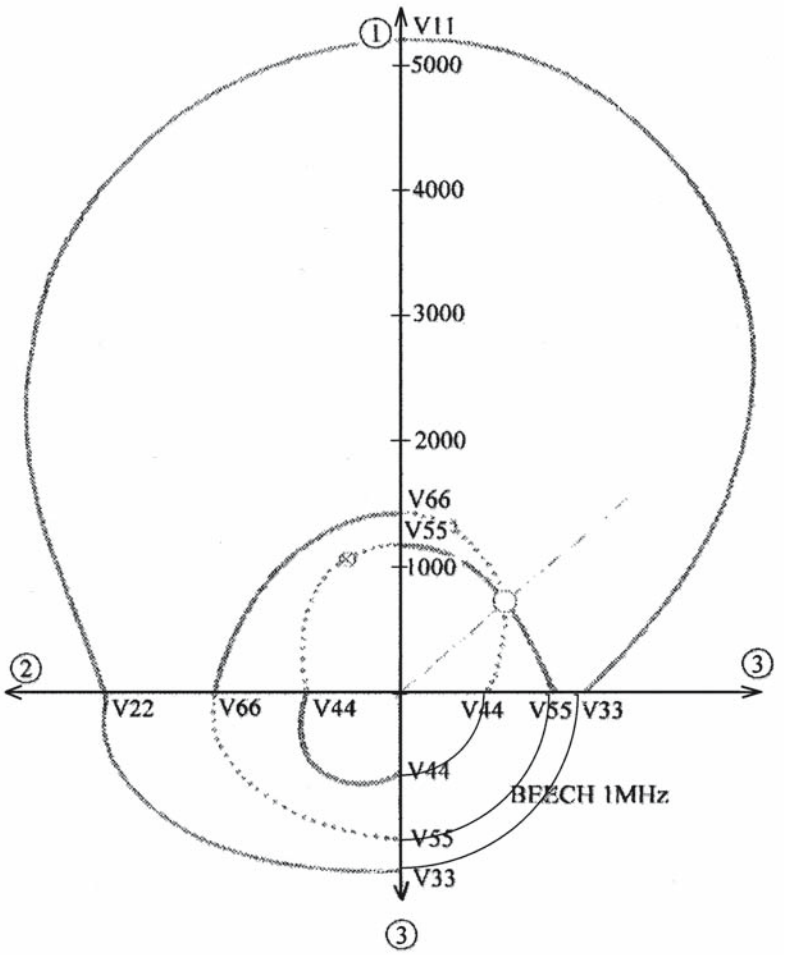

Fig. 4.2. Velocity surface of beech deduced from experimental values measured using broadband transducers that have a central frequency of 1 MHz

symmetry plane is often very accessible in practical situations. The anisotropy is more pronounced for Douglas fir than for oak, and leads to a large energy flux deviation of up to 45°. The QT wave mode in oak behaves almost like an isotropic mode, its phase velocities hardly changing with propagation angle. In oak, the energy flux deviations are quite small, not exceeding 12°; however, in Douglas fir, a strong maximum in the 60° propagation direction is observed. Mathematical modeling as well as practical experience show that the energy flux deviation of

Fig. 4.3. Slowness surfaces and wave surface of solids with orthotropic symmetry (uranium and spruce). **a** Uranium slowness surface in plane 13; **b** uranium wave surface in plane 13; **c** spruce slowness surface in plane 12; **d** spruce wave surface in plane 12. *QL* Quasi-longitudinal wave; *QT* quasi-transverse wave; *T* transverse wave. In the figures for spruce, the intercept of all the curves with coordinate axes should be at right angle. We should bear in mind that wood is not a perfect crystal and some deviations from the theoretical approach may be expected. (Musgrave 1970, with permission)

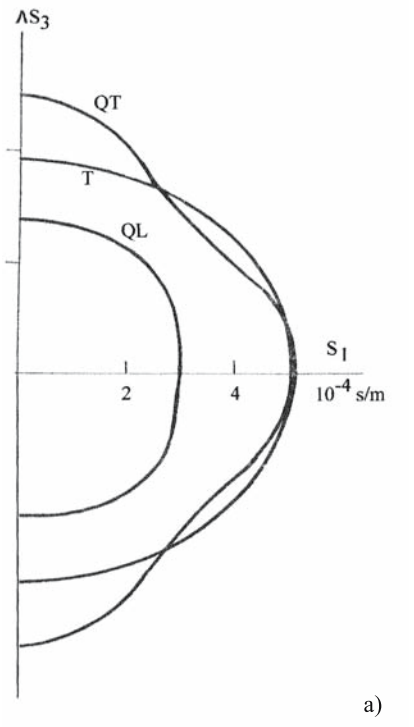
S3
QT
T
QL
S1
2
4
10^-4 s/m

a)

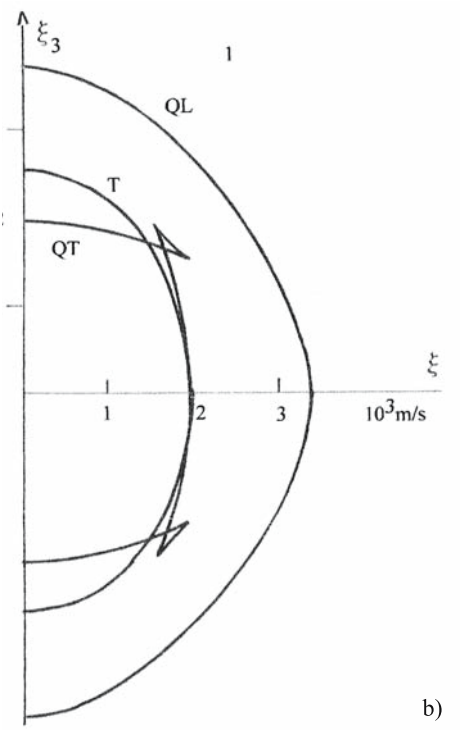
ξ3
1
QL
T
QT
ξ
1
2
3
10^3m/s

b)

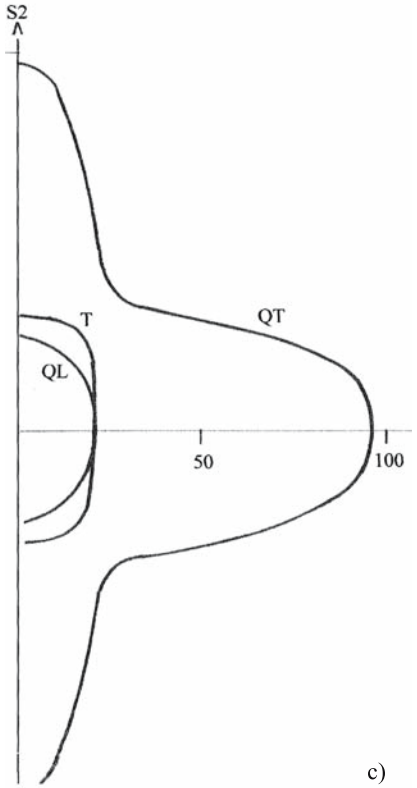
S2
T
QT
QL
50
100

c)

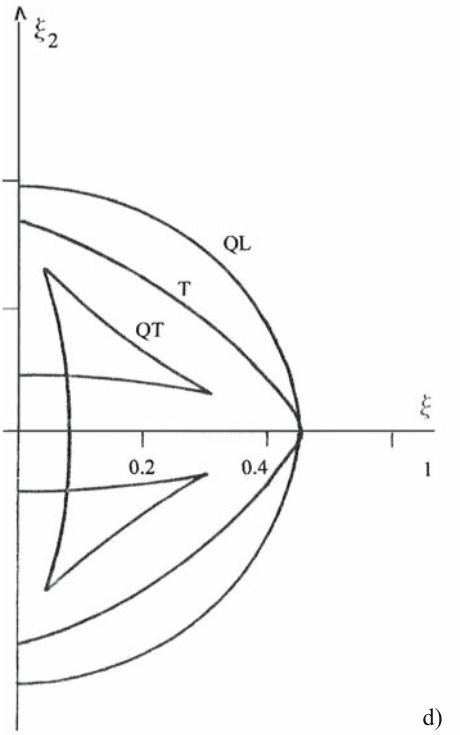
ξ2
QL
T
QT
ξ
0.2
0.4
1

d)

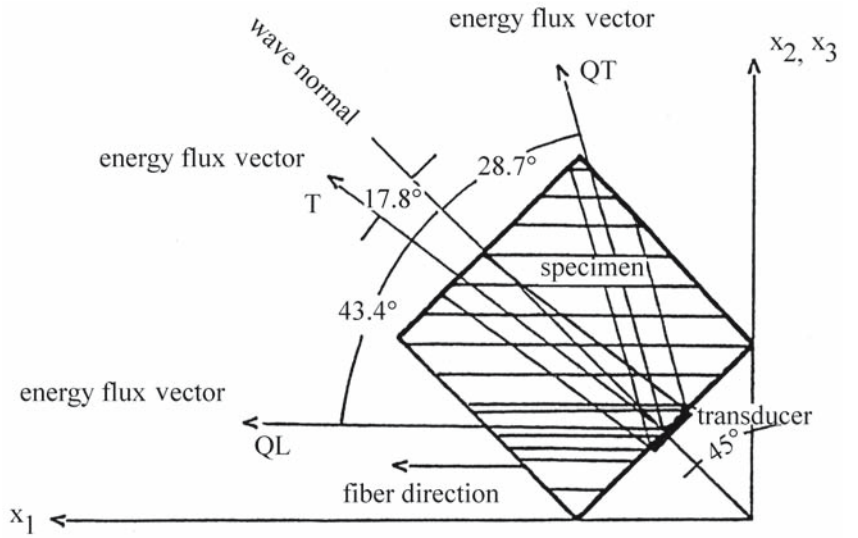

Fig. 4.4. Energy flux deviation in the X_1–X_2 plane in a transverse isotropic graphite fiber material. (Kriz and Stinchcomb 1979), with permission)

the QT wave is particularly sensitive to the magnitude of the off-diagonal elastic constants.

Acknowledging the phenomena of energy partition and energy flux deviation and adjusting the experimental design to take advantage of the additional measurable quantities will significantly improve the accuracy of ultrasonic determination of the off-diagonal elastic constants of wood.

4.2.1.2 The Eigenvectors of Christoffel's Equations

From Eq. (4.40) we can obtain the eigenvectors in a very simple way, if two off-diagonal components of the tensor are zero. In plane 12, for an orthotropic solid, the linear equation for the displacement P_m (p_1, p_2, 0) associated with the quadratic factor of Eq. (4.41) for (n_1, n_2, 0) is as follows:

$$(\Gamma_{11} - \rho V^2)\, p_1 + \Gamma_{12} p_2 = 0 \qquad (4.48)$$
$$\Gamma_{12} p_1 + (\Gamma_{22} - \rho V^2)\, p_2 = 0$$

where

$$p_1/p_2 = \Gamma_{12}/(\rho V^2 - \Gamma_{11}) = (\rho V^2 - \Gamma_{22})\,\Gamma_{12} \qquad (4.49)$$

If we let the polarization correspond to the same sign, i.e., $p_1 = \sin\beta$ and $p_2 = \cos\beta$, where β is the displacement angle, we obtain:

$$tg\beta = \Gamma_{12}/(\rho V^2 - \Gamma_{11}) \qquad (4.50)$$

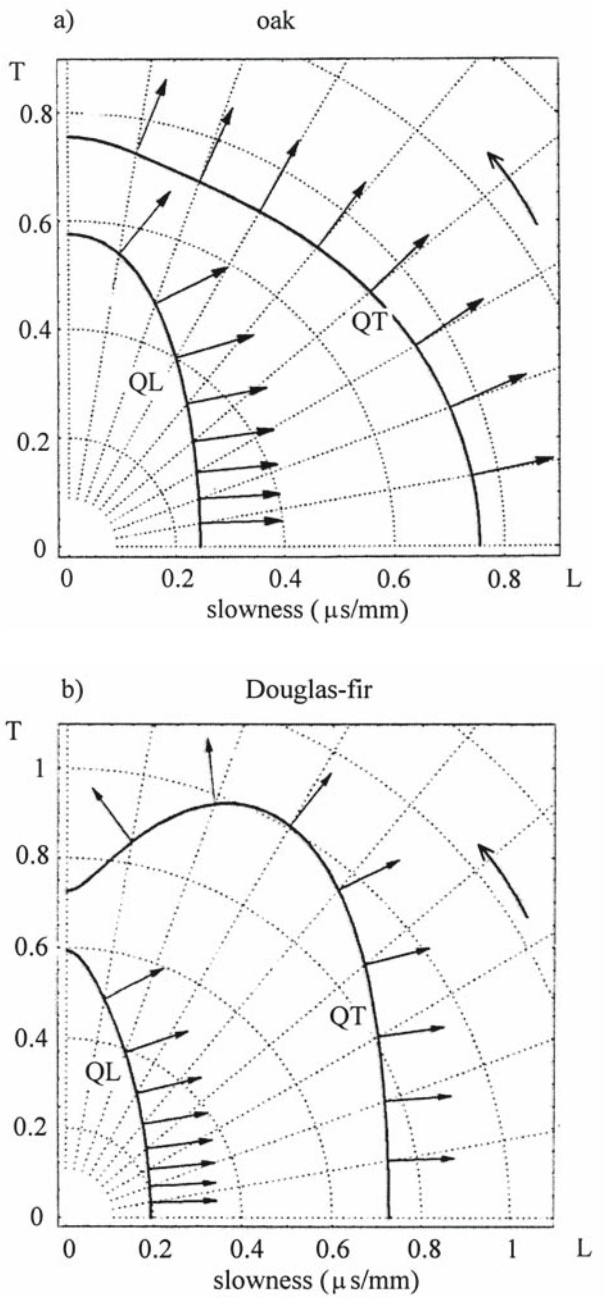

Fig. 4.5. The flux energy deviation angle and slownesses of QL and QT waves in **a** oak and **b** Douglas fir. (Bucur and Berndt 2001), with permission)

and

$$p_2 = cos\beta = (\rho V^2 - \Gamma_{11})/[(\rho V^2 - \Gamma_{11})^2 + \Gamma^2_{12}]^{1/2} \tag{4.51}$$

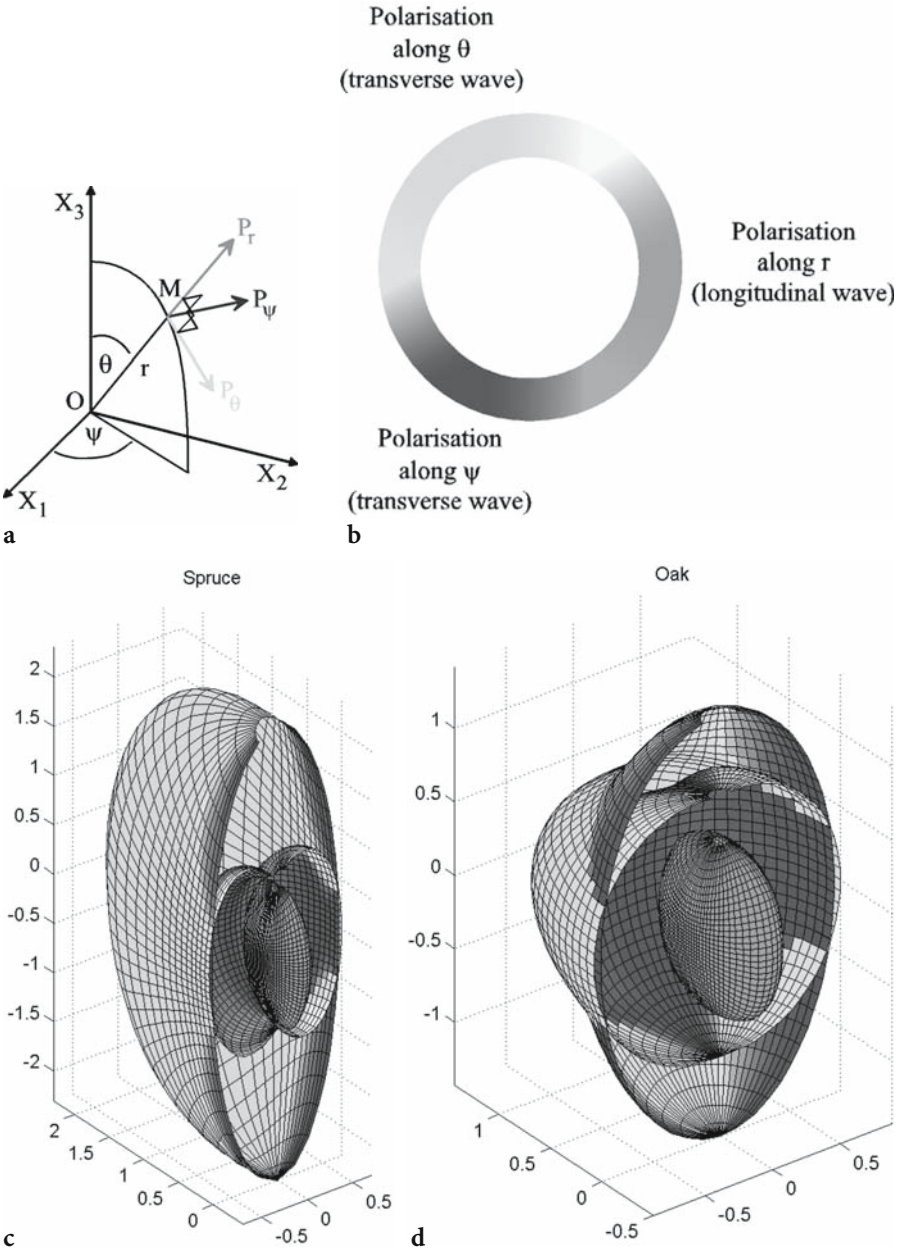

Fig. 4.6. Displacement field in wood. **a** Velocity surfaces in all anisotropic planes in spruce; **b** corresponding displacement fields represented by "tadpoles" (Kriz and Ledbetter 1986, with permission); **c** the polarization vector is decomposed along local spherical coordinates (Lanceleur et al. 1988, with permission); **d** tridimensional representation of slowness surface and corresponding displacements for spruce and oak (Bucur et al. 2002, with permission)

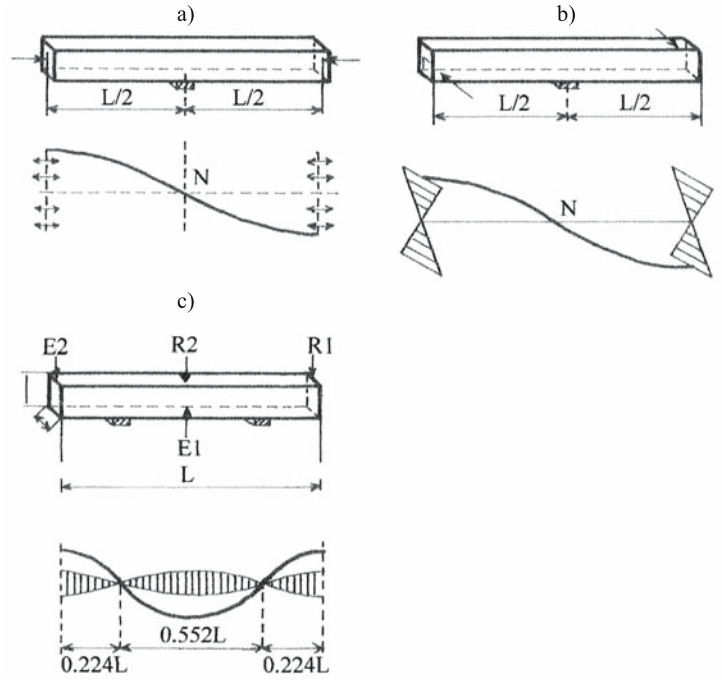

Fig. 4.7. Displacements at different vibration modes of bars. **a** Longitudinal vibrations in bars; **b** torsional vibrations in bars; **c** flexural vibrations. *N* Nodal point; *E* emission; *R* receiver. (Facaoaru and Jones 1971, with permission)

From Eq. (4.51) the particle displacement (polarization) is expressed in terms of phase velocity, propagation direction, and stiffness constants of the solid for each plane of symmetry. It can also be deduced that the polarization angle between the displacement vector belonging to the inner sheet of the slowness surface and the corresponding wave normal on the symmetry axis is 0°. On the axis the wave is a pure longitudinal wave . For pure shear waves, the angle between the propagation and polarization vectors is $\pi/2$. The polarization angle changes when the propagation direction is out of the principal directions. The displacement fields for spruce were represented by Kriz and Ledbetter (1986) by "tadpoles" for a relatively small number of angles (Fig. 4.6).

A better understanding of propagation phenomena in anisotropic solids is given by a tridimensional representation of slowness surfaces and corresponding displacements as suggested by Lanceleur et al. (1998) with a numerical modeling method. The polarization vector is decomposed along local spherical coordinates in three components, corresponding to the longitudinal wave and to two shear waves, QT and T, or fast and slow shear waves (Fig. 4.7). The anisotropy of spruce is more pronounced than that of oak. For both species the inner slowness sheets (QL, axis X_1 being the direction of the fiber) exhibited a flattened ellipsoidal shape; on the other hand, the external sheets for shear waves showed clear differences between species behavior in the acoustic field. This representation underlines kinematic aspects of wave propagation related to progressive mode conversion and expresses better in a global way the differences between species in their acoustical behavior.

4.2.2 Mechanical Vibrations in the Acoustic Frequency Range

The common audiofrequency acoustic methods for testing wood use frequencies below 20 kHz. Steady state or transient (impact) excitation can be used to test the dynamics at resonance vibration when elastic moduli are to be determined.

The direct, accurate measurement of engineering constants of wood (the three Young's moduli, the three shear moduli, and the six Poisson's ratios) is important in engineering and in product design. The most convenient technique for measuring these parameters with high precision depends upon measurements of the resonance frequencies of longitudinal, flexural, or torsional resonant modes of both a bar-shaped sample of circular or rectangular cross section and a plate sample. The fact that the technique is resonant ensures that frequency measurements will be highly precise. Self-consistency of data, related for example to Young's moduli, can be verified using the same bar-shaped sample with longitudinal and flexural resonant modes. The technique can be extended to measure the internal friction, if the quality factor Q or the logarithmic decrease are measured in addition to resonance frequency.

Experimental studies on the elasticity of solid wood and of wood-based composites are extensive and a very large number of techniques have been developed. Free oscillation methods and methods with forced vibrations, or resonance methods, have been used for measurements in a wide range of frequencies, ranging from 10^2 to 10^4Hz. The main disadvantage of the resonant technique is related to the shape of the specimen, rod or plate. It is well known that for solid wood it is easy to obtain rods or plates in LR or LT planes, but it is very difficult in the RT plane. Moreover, care must be taken to ensure that losses through the suspension system used to support the specimen are not significant compared to those intrinsic to the specimen (Kollmann and Krech 1960; Becker and Noack 1968; Kataoka and Ono 1975, 1976).

4.2.2.1 Resonance Vibration Modes in Rods and Plates

This section discusses the determination of the engineering constants of wood by resonance methods when the specimen is a rod or a plate. The most common vibratory resonant motions in a rod are longitudinal vibrations, flexural vibrations, and torsional vibrations. They are the dynamic counterpart of static tension, static bending, and static torsion.

We saw in Section 4.1 that for full characterization of a wood species, nine elastic constants and nine damping constants are required. On a rod cut in the principal direction L, R, or T of the material, only one Young's modulus and one shear modulus, with their corresponding damping constants, can be determined. On a thin quarter-cut plate four elastic constants together with four damping constants can be measured. These statements show the limitation of the mentioned technique. It is worth noting here that the main advantage of frequency resonance methods is related to the direct access by measurement to Young's moduli, shear moduli, and Poisson's ratios, as mentioned in several standard texts (Harris and Crede 1961; Hearmon 1961; Snowdon 1968; Cremer and Heckl 1973; Read and Dean 1978; Bodig and Jayne 1982; Vinh 1982).

Because the theoretical considerations related to the vibrational resonances in bars and plates have been analyzed in the reference books cited above and are

well known, only the final relationships between engineering constants and resonance frequency of different types of specimens are explored here.

For a homogeneous and nondispersive medium, the Young's modulus of a bar specimen can be deduced from the following equation:

$$E = 4\rho L^2 (f_{L,n}/n)^2 \tag{4.52}$$

where ϱ is the density, L is the length of the specimen, and $f_{L,n}$ is the frequency of the longitudinal mode (n=1). For other modes (n=2, 3, etc.) this relation must be corrected with specific coefficients.

Young's modulus can also be deduced from a flexural mode by the equation:

$$E = [4\pi^2 \cdot \rho \cdot \mathrm{L}^4 (f_{F,n})^2 \mathrm{A}]/\mathrm{I} \cdot \mathrm{k_i}^4 \tag{4.53}$$

where A is the area of cross section of the bar. Thus we have:

- For a circular cross section inertia momentum $I=\pi r^4/4$; where r is the radius of the cross section.
- For a square cross section $I=a^4/12$, where a is the width.
- For a rectangular cross section $I=bh^3/12$, where b is the width and h is the height.

The correction coefficient k_i is related to n mode. For the first mode k_i=4.730, for the second mode k_i=7.853, for the third mode k_i=10.996, etc.

The shear modulus can be deduced from torsional modes of bars of circular section, using the equation:

$$G = 4\rho \cdot \mathrm{l}^2 \cdot (f_n^T/n)^2 \tag{4.54}$$

where f_n^T is the torsional frequency of mode n (n=1, 2, 3, etc.).

Flexural modes at higher frequencies can be used for the simultaneous estimation of Young's modulus and shear modulus when the theory of a Timoshenko bar is applied. Figure 4.7 presents the displacements at different vibration modes of bars. When the vibration theory is used on a flat, thin quarter-cut plate, four wood elastic constants can be determined on a single specimen. The corresponding theory was developed by McIntyre and Woodhouse (1978, 1985, 1988) and by Caldersmith (1984).

4.2.2.2 Engineering Constants

Table 4.5 gives the Young's moduli of several species determined from the L, R, and T directions from longitudinal modes. The parameter measured was the resonance frequency.

The anisotropy of wood can be deduced from the values noted in Table 4.5, and may be expressed as the ratios of E_R/E_L lying between 7/100 and 16/100, or of E_T/E_L which lie between 5/100 and 9/100 and $E_L >> E_R > E_T$, as expected.

Longitudinal modes of vibration of the bar-type specimens were also used for purposes other than characterization of elastic behavior as follows:

- for estimating the elastic parameters of the fine structure of the cell wall (Sobue and Asano 1976; Tonosaki et al. 1983);

Table 4.5. Young's moduli in the principal directions of wood deduced from longitudinal vibrations at 11% moisture content, in the frequency range 4–21 kHz. *L*, *R*, and *T* are the principal symmetry axes of wood (*L* longitudinal direction, *R* radial direction, and *T* tangential direction versus the annual rings). (Ono and Norimoto 1985, with permission)

Species	Direction	Density (kg/m^3)	Young's moduli ($10^8 N/m^2$)	Anisotropy (%)
Sitka spruce	L	460	128	100
	R	449	9.09	7.42
	T	454	6.24	5.19
Lauan	L	481	118	100
	R	489	13.8	11.7
	T	478	6.38	5.40
Makoré	L	669	136	100
	R	673	21.58	15.8
	T	670	12.3	9.07
Matoa	L	795	194	100
	R	700	19.3	9.97
	T	674	11.4	5.58
Mizunara	L	630	120	100
	R	654	15.8	13.2
	T	620	9.69	8.09
Yachidamo	L	570	128	100
	R	548	13.6	10.6
	T	517	7.48	5.84

- for estimating the variation of the moisture content in wood (Tang and Hsu 1972; Suzuki 1980; Olszewski and Struk 1983; James 1986; Rebic and Srepcic 1988; Sasaki et al. 1988);
- for chemical modifications induced by acetylation and formaldehyde cross-linking (Norimoto et al. 1988; Akitsu et al. 1991);
- for genetic variations observed as differences in tree clones (Takada et al. 1989; Fujisawa et al. 1992).

Longitudinal vibrations can also be produced by the stress-wave method (Dunlop 1978, 1980; Gerhards 1982c) in which the velocity was the measured parameter. When frequency analysis is performed on the power spectrum of the stress-wave signal, it is possible to determine the resonance frequencies of different modes and consequently to compute instantaneously the Young's modulus on small clear specimens and on lumber of commercial size (the maximum reported dimensions are 20×20 cm×6 m and 114 kg). This very elegant approach was developed by Sobue (1986a,b,c) and involves tapping the specimen with a hammer and receiving the signal with a wireless microphone. A microcomputer connected to the system permitted the instantaneous treatment of data.

Flexural modes have been extensively used for the measurements of *E* on small clear specimens, especially for the characterization of wood for musical instruments. This approach is discussed in Chapter 7. Other interesting applications of flexural mode testing have been reported in the study of the anisotropy of plywood related to the disposition of the veneer sheets (Sobue and Ywasaki 1981a; Sobue 1983), the effect of adhesives on laminated lumber (Sobue

Table 4.6. Young's moduli E_L from different modes of vibration, determined at 12% moisture content. (Hearmon 1948)

Mode of vibration	Species	Density (kg/m^3)	E_L ($10^8 N/m^2$)
Bending of clamped specimen with additional mass	Beech	630	112
Longitudinal mode, free–free			117
Bending of clamped specimen with additional mass	Beech	710	121
Longitudinal mode, free–free			123
Bending of clamped specimen with additional mass	Pine	570	75
Longitudinal mode, free–free			82

Table 4.7. Dynamic Young's moduli determined by longitudinal and flexural vibrations in the LR plane at different angles for sitka spruce. 0° corresponds to the specimen in the L direction; 90° corresponds to the specimen in the R direction. (Tonosaki et al. 1983, with permission)

Angle	Longitudinal test (L)		Flexural test (F)		Ratio
(°)	F_L (Hz)	E_L^L ($10^8 N/m^2$)	F_F (Hz)	E_L^F ($10^8 N/m^2$)	E_L^L/E_L^F
0	9,531	141	581	138	1.02
15	9,530	68	943	58	1.17
30	6,194	15	612	25	0.60
45	4,906	16	472	15	1.06
60	4,269	18	410	11	1.63
75	4,057	19	382	10	1.90
90	3,797	19	359	9	2.11

and Ywasaki 1981b), and the mechanical properties of epoxy-poplar composite materials (Moore et al. 1983).

For testing purposes, the flexural mode offers the advantage of a relatively low frequency range, with $n=4$ or $n=5$, on specimens of reasonable length (30 cm). Table 4.6 gives values of Young's moduli, deduced by Hearmon (1948) from different testing configurations. Dynamic measurements with longitudinal modes give values higher by a few per cent than those from flexural modes. When measurements were performed out of principal directions (Table 4.7) the moduli determined from longitudinal modes were between 1.02 and 1.16 higher than those measured from flexural modes.

Flexural testing modes afford a very useful opportunity to observe the coupling effect between shear and extensional stress in wood. Dynamic methods of determining elastic constants, deduced from the flexural vibrations of beams, were developed by Sobue (1986b) on small clear specimens and on samples of commercial size such as logs (Sobue 1990; Arima et al. 1991) and timber (Sobue 1988, Chui 1991). Figures 4.8 and 4.9 show the complex vibrations of a plank struck with a hammer and the corresponding displacements for different modes. Specimens were tapped with the hammer at the edge, at an end, and at a point located one-quarter of the length from the end, to enhance the peaks of the higher harmonics. The tap tone was detected with two condenser micro-

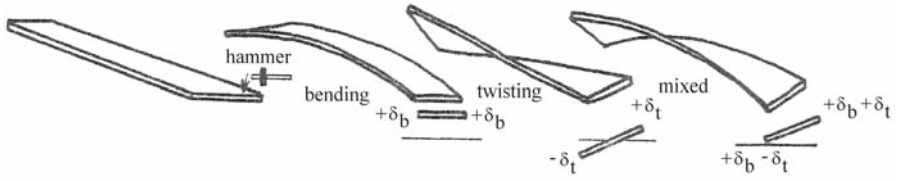

Fig. 4.8. Complex vibration of a plank struck with a hammer. (Sobue 1987, with permission)

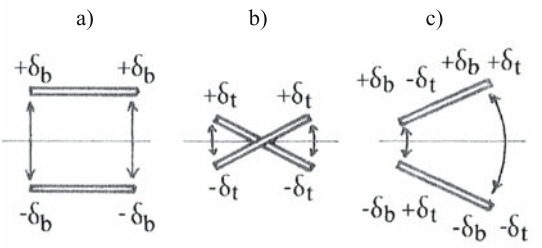

Fig. 4.9. Displacement of a beam seen in transverse section at different vibration modes. **a** Flexural mode; **b** twisting mode; **c** flexural and twisting mode. (Sobue 1988, with permission)

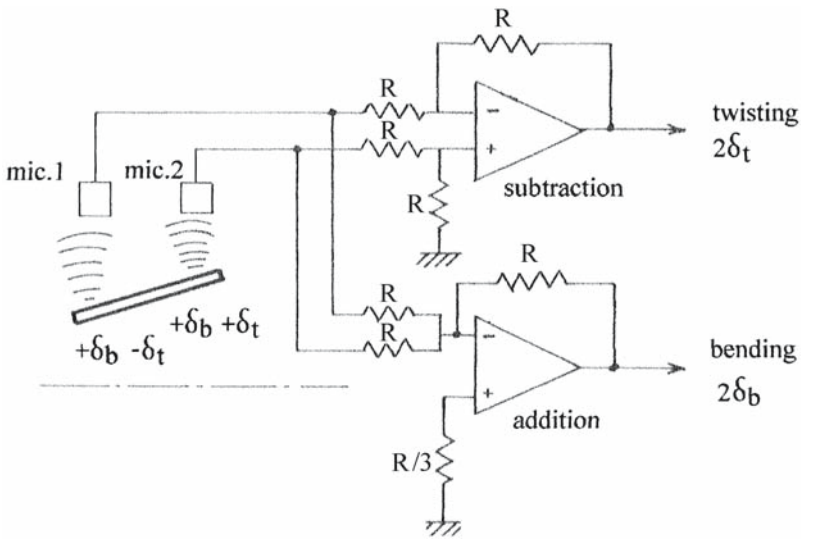

Fig. 4.10. Device used for the addition and subtraction of signals obtained from a plank struck with a hammer. (Sobue 1988, with permission)

phones, as can be seen in Fig. 4.10. A very sophisticated signal treatment with an FFT analyzer (Fig. 4.11) enabled the separation of peaks corresponding to flexural and twisting vibrations. The value of the frequency corresponding to each peak was determined precisely, and consequently the values of the elastic constants were deduced.

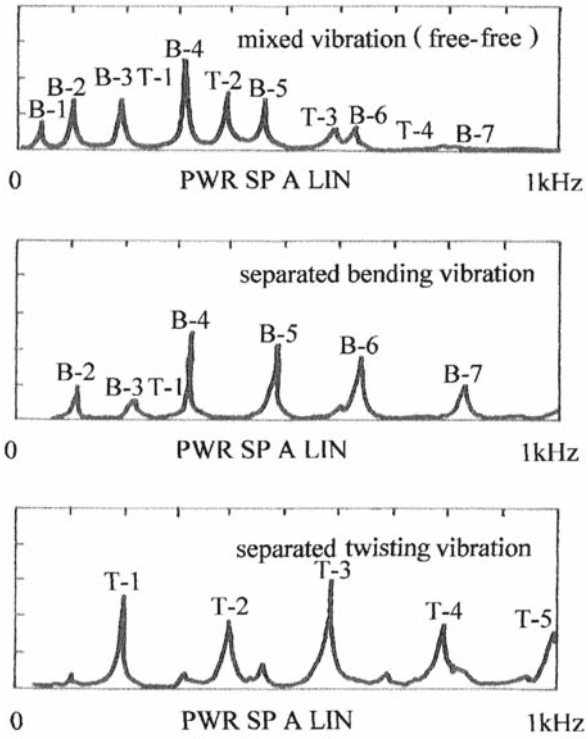

Fig. 4.11. Power spectra deduced from a board of lumber (dimensions 50 mm×100 mm×3 m). (Sobue 1987, with permission)

Among the resonance methods, the technique using the torsional mode with bar specimens (Becker and Noack 1968; Morze et al. 1979; Olszewski and Struk 1983) has been less used, probably because of practical difficulties related to the torsional pendulum and to the very small frequency band obtained during the testing. Some experimental difficulties could be overcome if we bear in mind that the temperature and frequency are equivalent parameters and a relatively low resonance frequency could be obtained by increasing the temperature of the specimen.

Becker and Noack (1968) published an interesting study on beech, which gave the relationship between shear modulus, temperature variation (20...100 °C), and moisture content (5...30%) in order to characterize the viscoelastic behavior of wood, as can be seen in Fig. 4.12.

Another way to determine the elastic constants of wood is to use plate vibration tests on which complex Young's moduli, shear moduli, and Poisson's ratios can be determined, as shown by Caldersmith and Rossing (1983), Nakao et al. (1985), Tonosaki and Okano (1985), McIntyre and Woodhouse (1988), Schumacher (1988), Molin and Janson (1989), Sobue and Katoh (1990), and Sobue and Kitazumi (1991).

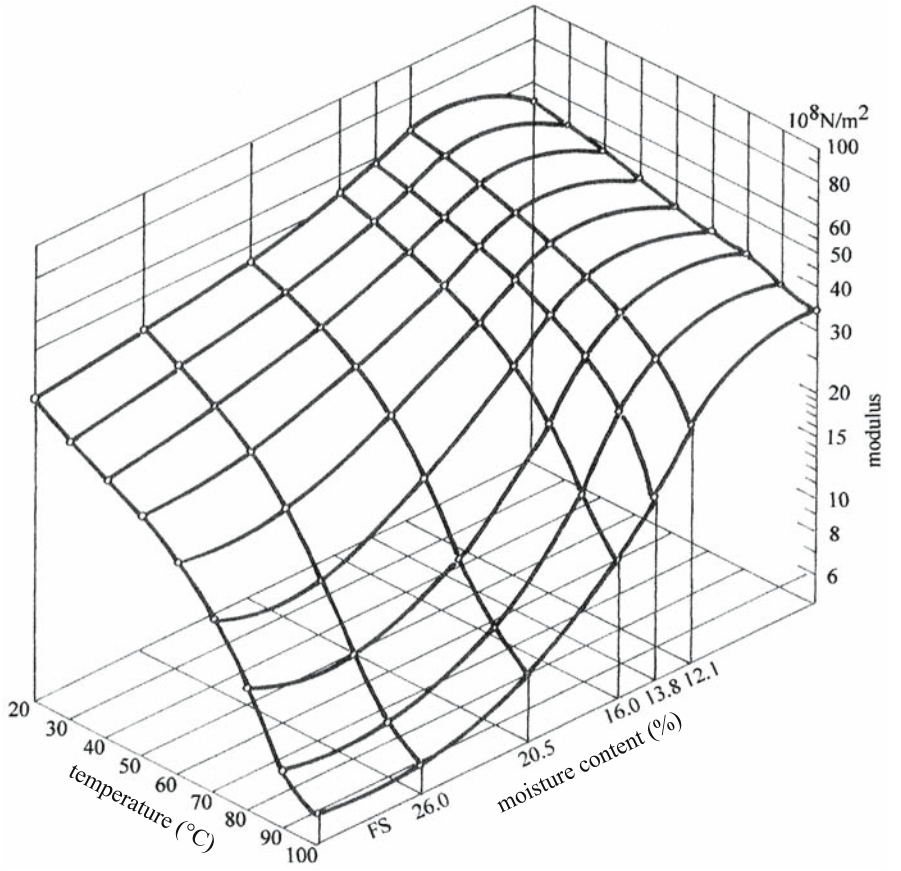

Fig. 4.12. Influence of temperature and moisture content on the shear modulus in beech. *FS* Fiber saturation point. (Becker and Noak 1968, with permission)

On orthotropic plates the resonance frequencies $f_{r(i,j)}$ are related to the elastic parameters by the equation:

$$f_{r(i,\,j)} = \tfrac{1}{2}\pi\,[S'/\rho h]^{1/2} \tag{4.55}$$

and

$$S' = D_{11}a_{1(ij)}a^{-4} + D_{22}a_{2(ij)}b^{-4} + 2D_{12}a_{3(ij)}a^{-2}b^{-2} + 4D_{66}a_{4(ij)}a^{-2}b^{-2} \tag{4.56}$$

where ϱ is the density of the material, h is the height, a is the length, and b is the width of the plate, $a_{1(ij)} \ldots a_{4(ij)}$ are coefficients depending on the supported condition of the plate (clamped, free, or simply supported), D_{11}, D_{22}, and D_{12} are flexural rigidities and D_{66} is the torsional rigidity. Table 4.8 gives the coefficients for the most common experimental condition, the free vibration mode.

Table 4.8. Values of coefficients a_1–-a_4 from Eq. (4.56) for a completely free vibration of a rectangular orthotropic plate. $X=(m-0.5)\pi$ and $Y=(n-0.5)\pi$. (Sobue and Kitazumi 1991, with permission)

Vibration modes		Coefficients			
m	n	a_1	a_2	a_3	a_4
1	1	0	0	0	144
0	2	0	500.6	0	0
0	3, 4, etc.	0	Y^4	0	0
2	0	500.6	0	0	0
3, 4, etc.		X^4	0	0	0
1	2	0	500.6	0	593.76
1	3, 4, etc.	0	Y^4	0	12.3Y(Y+6)
2	1	500.6	0	0	593.76
2	2	500.6	500.6	151.3	2448.3

The engineering constants, Young's moduli, shear modulus E_1, E_2, and G_{12}, and Poisson's ratio ν_{12} in the corresponding anisotropic plane (i.e., 12) can be calculated by the following equations:

$$E_1 = 12h^{-3}D_{11}(1 - D^2_{12}/D_{11}D_{22}) \tag{4.57}$$

$$E_2 = 12h^{-3}D_{22}(1 - D^2_{12}/D_{11}D_{22}) \tag{4.58}$$

$$G_{12} = 12h^{-3}D_{66}(1 - D^2_{12}/D_{11}D_{22}) \tag{4.59}$$

$$\nu_{12} = D_{11}/D_{22} \tag{4.60}$$

Based on these theoretical assumptions, Sobue and Kitazumi (1991) precisely determined the resonance frequency of a rectangular free vibrating plate, identifying the corresponding peaks from the power spectrum of different vibration modes (i.e., [0,2], [1,1], [2,0], [2,2]). Figure 4.13 gives the typical power spectrum of a Western red cedar plate (300×300×10 mm). The misidentification of peaks corresponding to flexural or torsional modes was avoided since the phase of deflection was considered. The proposed procedure was used for the automatic identification of resonance peaks of the power spectrum and consequently for simultaneous, routine measurements of engineering constants E_1, E_2, and G_{12}.

4.3 Velocity of Ultrasonic Waves in Wood

The measurement of ultrasonic wave velocities in wood, considered as an orthotropic material, is the basis of the nondestructive evaluation of its elastic or viscoelastic properties.

The fundamentals of the propagation of ultrasound in homogeneous solids are given in McSkimin (1964) and in Papadakis (1990) in polycrystalline media. Given the existence of these excellent references the emphasis in this section is on theoretical aspects which are related directly to the measurement techniques appropriate for wood.

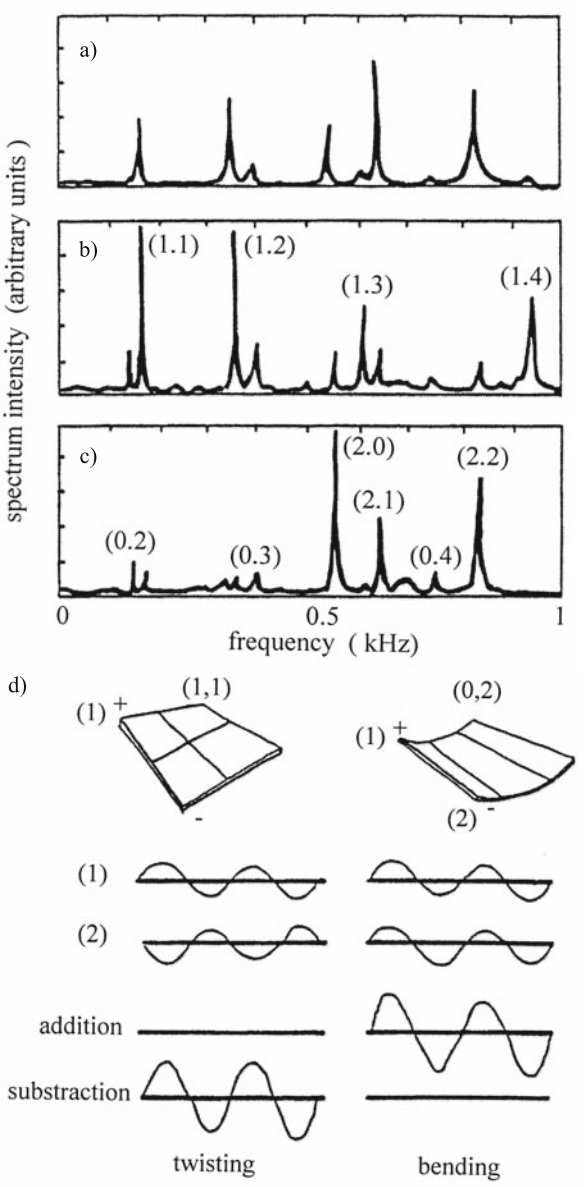

Fig. 4.13. Power spectra on a rectangular freely vibrating western red cedar plate. **a** Detected by the microphone; **b** separated by the subtraction procedure for twisting modes; **c** separated by the addition procedure for flexural modes; **d** vibrational modes of the plate. (Sobue and Kitazumi 1991, with permission)

The principal wave types used for measuring wood properties are the bulk waves (longitudinal or transverse-shear) and surface waves (Rayleigh, Lamb, and Love waves). The waves are characterized by the direction of propagation and by the particle motion, i.e., for longitudinal waves the particle trajectory is in the direction of propagation, for transverse waves the particle motion is perpendicular to the direction of propagation; for Rayleigh waves the particle trajectory is elliptical in the plane that is perpendicular to the tested surface and parallel to the direction of propagation.

In dispersive media the ultrasonic velocity is dependent on frequency, and both phase and group velocities (or the velocity of the wave packet) can be measured. The relationships between group velocity v and phase velocity V have been extensively commented on by Guilbot (1992) and can be summarized by the equation:

$$v=\frac{V}{\left(1-\frac{f}{V}\cdot\frac{dV}{df}\right)} \tag{4.61}$$

The phase velocity is

$$v=\frac{\omega}{k}=f\cdot\lambda \tag{4.62}$$

where $\omega=2\pi\times f$ and f is the frequency, the propagation constant is $k=\frac{2\pi}{\lambda}$, and λ is the wavelength. When $k=k(\omega)$ and when also V is a function of frequency, the medium is dispersive. Dispersion may be induced by the geometry of the specimen, the nature of the material, the scattering produced by the inhomogeneities of the structure, the absorption of wave energy by the material during propagation, etc. Experimental methods for the determination of phase and group velocities in dispersive solids are given in Sachse and Pao (1978) and Sahay et al. (1992).

4.3.1 Measurement System

Ultrasonic velocity measurements can be taken from broadband pulses or narrowband bursts and are related to the measurement of time of flight and length of specimen. Either the immersion technique (when the specimen is immersed in a liquid) or the direct transmission technique (when the specimen is in contact with the transducer) can be used for wood material. The immersion technique is more appropriate for laboratory testing, while the direct transmission technique is convenient for both laboratory and field measurements. The principal advantage of either technique is the flexibility in measuring velocity and attenuation of ultrasonic waves.

Wood material that is to be sensed and probed with ultrasonic waves may be most conveniently divided into three main groups: trees and logs, small clear specimens of solid wood, and wood-based composites and engineering products. The direct transmission technique seems to be the most generally appropriate technique for ultrasonic testing of all these types of wood.

4.3.1.1 Devices

The most usual block diagram for ultrasonic velocity and attenuation measurements is presented in Fig. 4.14. The electrical signal is transmitted from the generator to the emitter (E), transducer to E, and transformed into an ultrasonic pulse. This pulse travels through the specimen and is received by the receiver (R), transducer to R, and is transformed again into an electric signal which is visualized on an oscilloscope. This allows the measurement of the time elapsed between emission and reception. The time delay is measured on the oscilloscope, over the path length of the ultrasonic signals. The technique is very simple and

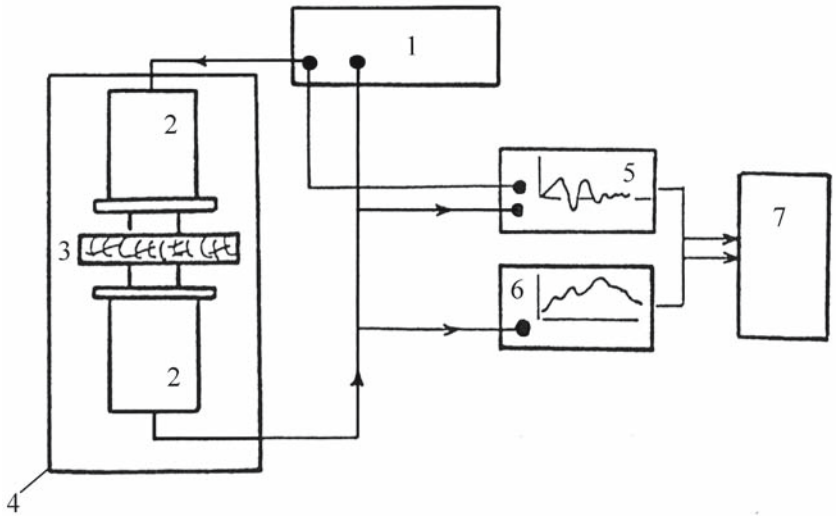

Fig. 4.14. Block diagram for velocity and attenuation measurements using the direct transmission technique. *1* Ultrasonic generator; *2* transducer; *3* specimen; *4* mechanical device; *5* oscilloscope; *6* spectrum analyzer; *7* computer. (Bucur and Böhnke 1994, with permission)

the time measurements very accurate (error less than 1%). For more sophisticated measurements related to attenuation or phase, a spectrum analyzer can be used.

4.3.1.2 Transducers

The physical basis for the generation and detection of ultrasonic signals with piezoelectric transducers has been extensively commented on in books and articles on physical acoustics (Sachse and Hsu 1979; O'Donnell et al. 1981; Lynnworth 1989; Hutchins and Hayward 1990; Hamstad 1997; Schmerr 1998; Papadakis 1999). In the ultrasonic generation mode, the transducer incorporates a piezoelectric element which converts electrical signals into mechanical vibra-

Table 4.9. Acoustic and piezoelectric parameters of piezoelectric materials for ultrasonic transducers. (O'Donnell et al. 1981, with permission)

Symbol	Parameter
d	Transmission constant (strain out/field in)
g	Receiving constant (field out/stress in)
ϱ	Density
V^2	Ultrasonic velocity in a particular direction
Zo	Characteristic acoustic impedance
ε^T	Free dielectric constant (unclamped)
K_T	Electromechanical coupling efficiency
Q_m	Mechanical quality factor

Table 4.10. Piezoelectric material properties for longitudinal and transverse waves. *Quartz** Quartz 0 X-cut; *Quartz 1* quartz 0 Y-cut; *Quartz 2* AT cut; *AT* thickness of shear cut when the quartz plate orientation is considered. Mode of vibration of crystalline piezoelectric material is determined by orientation of plate relative to crystalline axes. (O'Donnell et al. 1981, with permission)

Symbol	Units	Longitudinal waves					
		Quartz*	PZT-4	PZT-5	PZT-H	$PbNb_2O_6$	$BaTiO_2$
d	10^{-12} m/V	2	289	374	593	75	149
g	10^{-3} Vm/N	50	26	25	20	35	14
ϱ	kg/m^3	2.50	7,600	7,500	7,500	5,900	5,700
V^2	m/s	5,650	3,950	3,870	4,000	2,700	4,390
Zo	10^4 kg/m^2	15	30	29	30	16	25
$\varepsilon^T/\varepsilon^0$	–	4	1,300	1,700	3,400	240	1,700
k_T	%	11	70	70	75	40	48
Q_m	–	<22,5000	<500	<75	<65	<5	<400
Symbol	Units	Transverse waves					
		Quartz 1	Quartz 2	PZT-4	PZT-5	PZT-5H	$BaTiO_2$
d	10^{-12} m/V	4.4	3.4	496	584	741	260
g	10^{-3} Vm/N	110	80	38	38	27	20
ϱ	kg/m^3	2,650	2,650	7,600	7,500	7,500	5,700
V^2	m/s	3,850	3,320	1,850	1,680	1,770	2,725
Zo	10^4kg/m^2	10	9	14	13	13	16
$\varepsilon^T/\varepsilon^0$	–	5	5	1,475	1,730	3,130	1,450
k_T	%	14	9	71	68	65	50
Q_m	–	>2,500	>25,000	<500	<75	<75	<300

tion. The inverse effect is used for the detection of ultrasonic waves traveling through the specimen.

The active element in a piezoelectric transducer is a disk, made from such ceramic materials as barium titanate, lead zirconate-titanate, lead metaniobate, etc., which have a favorable combination of mechanical, electrical, and piezoelectric properties. Some data on the acoustic and piezoelectric parameters of materials used for ultrasonic transducers are given in Tables 4.9 and 4.10. The mode of vibration of piezoelectric ceramics (longitudinal shear, etc.) is determined by the orientation of the disk relative to an axis that is imposed onto the material during the sintering process. The polarization of the structure is achieved by first raising the temperature of the ceramics above the Curie point and then cooling the ceramics in a strong electric field.

The dimensions and shapes of several transducers commonly used for velocity and attenuation measurements in the 1980s and 1990s are given in Fig. 4.15. The time domain and frequency domain response of a 1-MHz broadband transducer are shown in Fig. 4.16.

The performance of transducers is related to their constructional parameters such as the radiation surface area, mechanical damping, the characteristics of the piezoelectric and backing materials, and the connection of electrical and acoustical components of the system. The choice of the piezoelectric material is dictated by the specific application required by the transducers, as can be seen from Tables 4.9 and 4.10. The efficiency as a transmitter is related to a large "d"

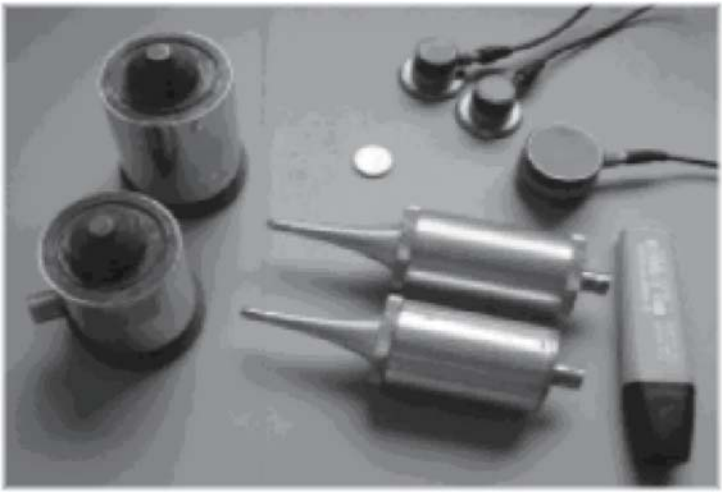

Fig. 4.15. Sample broadband ultrasonic transducers for ultrasonic and attenuation measurements using the direst transmission technique. (Courtesy of Panametrics Inc., Waltham, Maryland)

constant, whereas the sensitivity as a receiver is more dependent on a large "g" constant.

The basic requirements of an ultrasonic transducer are good sensitivity and resolution, controlled beam pattern, and reproducible performance under various testing conditions and high signal to noise ratio. The source of many experimental limitations associated with piezoelectric transducers is the coupling medium with the specimen under test. Very often the ultrasonic signal is disturbed and interference phenomena, phase shift, and attenuation of the signal are associated with the propagation in the coupling layer. Further comments on this subject are given in the following section.

Development of noncontact ultrasonic sensing using air or gas (Anderson et al. 1994) coupled transducers for industrial applications began around 1996, when several laboratories developed transducers to test solids with impedance in the range $V \times \rho = 1{,}500$ m/s$\times 1$ kg/m$^3 = 1.5 \times 10^6$ kg/m^2, for example plastics, foamy plastics, wood, and liquids. Typical applications included object presence detection, height differentiation, measuring position, level measurement in bins, silos, level of water, registration of people, automatic door-openers, control of fine-arts objects (Grandia and Fortunko 1995; Papadakis 1999; Green 2001), particleboard blow detectors operating in the 25-kHz range (Birks 1972), measurements in gases (Gallego-Juarez et al. 1978), inspection of reinforced ceramics (Stoessel et al. 2002), estimation of material quality when velocity or density cannot be measured, and measurements at elevated temperatures (Bharadwaj et al. 2000).

4.3.2 Specimens for Ultrasonic Testing

It is appropriate to observe that measurements of ultrasonic velocity and attenuation are influenced by requirements related to sample preparation, to the coupling of the transducer to the sample, and to the refined signal processing. This

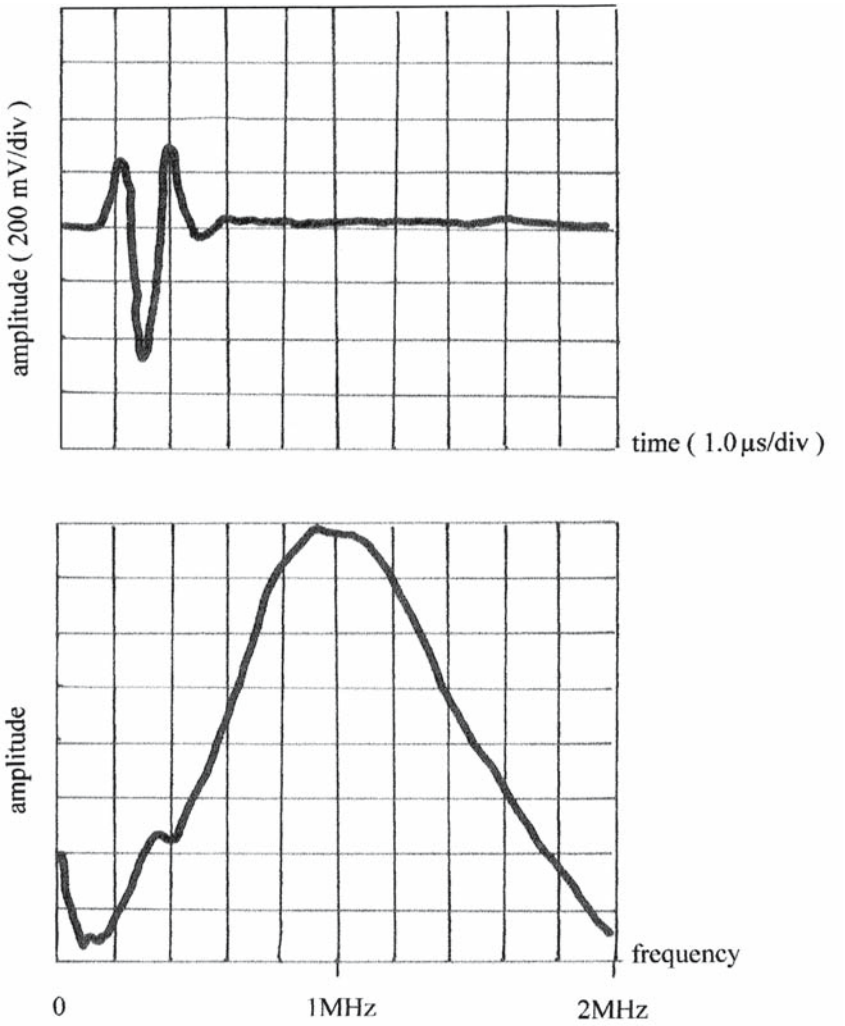

Fig. 4.16. Time and frequency domain response characteristics of a 1-MHz broadband transducer. (Courtesy of Panametrics Inc., Waltham, Maryland)

section reviews some of the specific requirements for testing trees, small clear specimens, and wood-based composites.

4.3.2.1 Preparation of Samples

In the term "samples" we include all type of wood specimens such as trees, small clear specimens of solid wood, and wood-based composite specimens. The specific differences in the requirements of preparation of particular samples are discussed later.

Ultrasonic measurements of trees may be performed on the periphery of the trunk, with or without bark (Bucur 2003a). Measurements of logs can be carried

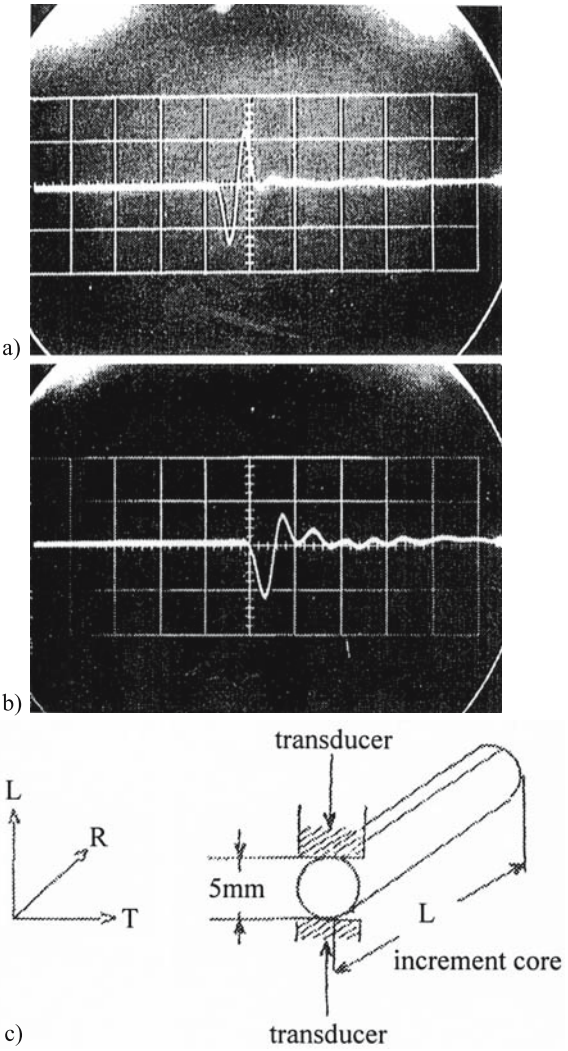

Fig. 4.17. Pulse shape displayed when propagation of a 1-MHz signal in a 5-mm Douglas fir increment core occurs in the longitudinal direction. **a** Signal with the transducers in contact; **b** signal with increment core; **c** increment core for testing. (Bucur 1984a)

out on the transverse sections at both ends. In this case no specific care is needed, although the surfaces must be parallel and as flat as possible.

The potential of the ultrasonic velocity method has been demonstrated in the nondestructive measurement of the slope of the grain of living trees and when qualitative parameters for round wood were established (see Chap. 8). The range of ultrasonic velocities measured in wood at 12% moisture content at 1 MHz is between 6,000 m/s for longitudinal waves in the fiber direction and 400 m/s for shear waves in the radial-tangential plane. The values of the attenuation coefficients are roughly 2 dB/cm for longitudinal waves in the fiber direction and 15 dB/cm for shear waves in the transverse anisotropic plane.

The conditions for satisfactory specimen preparation depend essentially on the magnitude of attenuation of ultrasonic waves in the wood species under test. Generally the higher the attenuation, the greater the requirements concerning the flatness and parallelism of the specimen surfaces. In addition, the samples must

be accurately perpendicular to the principal direction or to the required direction out of the main symmetry axes along which the ultrasonic waves propagate. The geometric shape of typical small clear wood specimens used for acoustical measurements may be a rectangle, parallelepiped, cube, rod, multifaced disk, plate, polyhedron, or sphere . The choice of one of the geometrical shapes for the specimens is determined by the purpose of the research. Generally speaking, use of the ultrasonic immersion technique necessitates plates or spheres, while any specimen shape is suitable for the direct contact technique. If wave velocities are of interest along only a restricted range of directions (commonly the longitudinal direction), then the minimum requirement for specimen preparation is to have two-plane, parallel faces. The larger the specimen dimensions, the longer the propagation time of the ultrasonic signal in wood, and the higher the accuracy of measurement.

At relatively high frequencies the requirements on parallelness of the opposite faces of wood specimens become more severe and the bond between the transducers and the sample becomes more critical. In wood science literature, velocity measurements in the longitudinal direction have been reported for a very large range of dimensions, varying from the millimeter scale (Bucur 1984a) to meters (McDonald 1978).

Figure 4.17 shows the pulse shape displayed by propagation of a 1-MHz signal in a 5-mm-thick Douglas fir increment core in the longitudinal direction. In such an extreme case, attention should be paid to the excitation of the ultrasonic pulse and, if necessary, to the repetition rate, as well as to the excitation pulse length.

Errors may be introduced into the velocity measurements if the arrival time of the distorted pulse is compared with that of the undistorted pulse when the probes are in contact. The misalignment of the transducers and specimens is another important introduced error. The error becomes larger when the sample is not accurately aligned with the transducer. One procedure used to diminish this effect is to maximize the amplitude of the signal from the interface.

If all the elastic stiffnesses of a wood species are required, the sample size and shape constraints are more severe. In laboratory measurements, we need to manipulate rather small specimens, to limit the effect of any spatial inhomogeneity of wood induced by its anatomical structure, and to allow the annual ring curvatures related to the T direction to be neglected. However, the specimen that would be used for the measurements of the nondiagonal terms of the stiffness matrix does allow the propagation of quasi-longitudinal and quasi-shear waves out of principal symmetry axes. The specimen and ultrasonic beam must be rotated relatively to each other. This may be done in several ways, e.g., (1) the ultrasonic beam may be rotated with respect to a fixed sample which has (or which has no) edges that coincide with the material symmetry axes; and (2) the ultrasonic beam is held in a fixed position while the specimen cut off-axis is rotated.

The first method is typically used in the immersion technique in which plate-type specimens (45×45×10 mm) are used (Preziosa et al. 1981). Commonly three plates, one corresponding to each anisotropic plane, are employed for the characterization of a wood species. The utilization of a sphere with the immersion technique, as a unique specimen for the measurement of all stiffness terms, avoids the natural variability introduced by the utilization of several specimens for the characterization of one species and has been demonstrated by Bucur and Rasolofosaon (1998). In the second method, used together with the direct contact technique, cubic specimens, multifaced disks, or polyhedral specimens are employed.

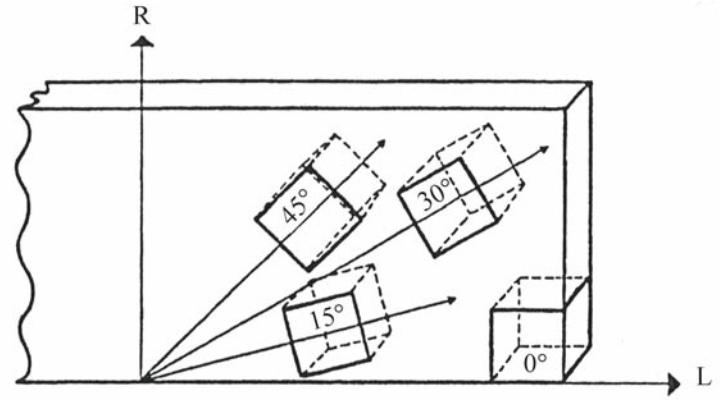

Fig. 4.18. Rotation of a cubic specimen in the LR plane. (Bucur 1984a)

The oldest method for the determination of effective elastic constants of composites is to cut cubes at specific angles with respect to the principal directions and to measure the corresponding velocities (Zimmer and Cost 1970; Rose et al. 1991a,b). Figure 4.18 shows the rotation (0, 15, 30, and 45°) of a cubic specimen with 16-mm sides in the LR plane, cut from a wooden plate. The same cubes were used to measure the velocities at 105°, 120, and 135°. Ten cubes were necessary for the determination of the terms of the stiffness matrix of one wood species (Bucur and Archer 1984). The cubic shape of the specimens should not present technical difficulties in the cutting process, but the great number of samples caused some practical difficulties.

In order to avoid this very tedious procedure and to restrict the natural variability of specimens, a multifaced disk sample could be use (Fig. 4.19). The diameter of the disk is 35 mm. The faces are cut at 15°, 30°, 45°, and 75° as well as at 0° and 90° (Bucur and Perrin 1988a). For experimental efficiency and economy of sample material and of time producing specimens, the disks seem to be an efficient sample type for ultrasonic measurements using the direct contact technique. Only three disks are needed for the complete characterization of a wood species. Improvement of this approach has been suggested by François (1995, 2000) who used only one polyhedral specimen with 26 faces for the measurement of 21 terms of stiffness tensor. Bucur and Rasolofosaon (1998) used a sphere of 5 cm diameter in the immersion technique and about 100 directions of propagation were ausculted for velocity measurements.

The influence of the natural variability of specimens, due to the biological nature of wood, on velocity and attenuation may be studied by choosing the frequency of the source so that the acoustic wavelengths in the material lie in a range roughly between the maximum dimension of the anatomical elements and the minimum specimen dimension. Some comments on the accuracy of the results of velocity and attenuation measurements are appropriate here. Parameters such as the probe diameter, the maximum pulse width, the attenuation of the ultrasonic wave in wood in the principal three anisotropic planes, and the separation time of quasi-longitudinal and quasi-transverse waves need to be considered when determining sampling strategy. Deviation of the energy flux vector of the quasi-longitudinal and quasi-transverse waves should not be ignored when determining the size of the specimen to be tested. A second consequence of the

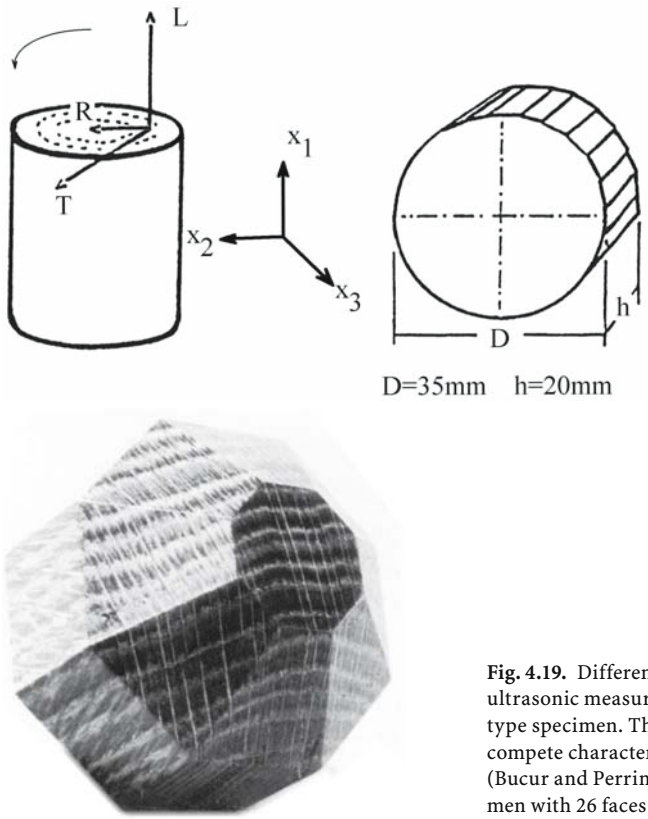

Fig. 4.19. Different types of specimens for ultrasonic measurements . **a** Multifaced disk-type specimen. Three disks are needed for compete characterization of a wood species (Bucur and Perrin 1987). **b** Polyhedral specimen with 26 faces (François 1995, 2000)

energy flux deviation is that for certain directions out of the principal axes, the propagation of more than three modes can occur. This phenomenon must be accounted for in order to avoid misinterpretation of the readings.

However, in anisotropic and inhomogeneous materials such as wood, a mechanical transducer will generate multiple modes simultaneously. This phenomenon is of special consequence to the ultrasonic investigation of thin specimens in the RT plane, since the repetition rate of the pulse is too great to allow the various modes to be separated in time. Consequently, misinterpretation of travel time or attenuation measurements can occur.

A lower limit to the size of the specimen is also imposed by the requirement that waves should have the character of plane waves in an infinite medium. The minimum size of the specimen ($<2\lambda$) must be established experimentally, since no good theoretical criterion exists for this purpose.

The presence of inhomogeneities in a sample limits the achievable accuracy of the readings. For example, in a sample where internal cracks or other discontinuities are comparable with the pulse wavelength, the pulse is attenuated by scattering at interfaces. The attenuation is frequency dependent if the pulse shape is changed, and errors in velocity and attenuation readings can occur. If the size of the discontinuities is much smaller than the wavelength, the change in pulse shape is smaller, allowing accurate data to be obtained. If inhomogeneity arises because of a gradual change in the measured property with position in a sample

(caused perhaps by decay or other biological attack), then the wave velocity in a particular direction varies with the part of the specimen through which the ultrasonic pulse is traveling. Changes in the measurements of velocity or attenuation would indicate the degree to which the sample was inhomogeneous in different zones.

This is a good place to drawn attention to the fact that other factors, such as internal and external conical refraction of the ultrasonic beams and the noncoincidence of pure mode axes with the symmetry directions, need to be investigated further. However, the complexity discussed above needs to be taken into account as regards the most frequently used configuration, which consists of sending an ultrasonic wave in the direction parallel to the axis L.

Finally, it is worth remembering that the main advantage of using ultrasonic waves on wood specimens to measure velocities and attenuations is that the material under test is not affected by the propagation phenomena. The sample can be retested because no deformation or destruction occurs. The ultrasonic tests can be repeated on the same sample and show little variation. The results may be repeated for similar samples and experimental conditions.

4.3.2.2 Coupling Media

Commercially available ultrasonic transducers are constructed with a layer of material covering and protecting the piezoceramic element. Vincent (1987) and D'Souza et al. (1989) have dealt with the specific effects of coupling and matching layers on the efficiency of ultrasonic transducers. Several types of coupling from transducer to sample are possible, as well as several arrangements of the transducers with respect to the specimen (Truell et al. 1969). A single transducer can be both the source and the receiver for the echoes that result from a single pulse. Alternatively two transducers on the opposite faces of the specimen can be used separately as emitter and receiver of an ultrasonic pulse. In the particular case of small clear wood samples^, the most suitable scheme seems to use two transducers. The scheme with a single transducer may be used only if the specimen does not exhibit too much attenuation. The limits depend on the thickness of the sample and its specific attenuation, which is most important in the RT plane.

In this section, attention is given first to the coupling media used with wood specimens in the direct transmission technique with two transducers. Coupling media are necessary to ensure the bonding of the transducer to the wood specimen. This is accomplished using a variety of materials (solids or liquids), depending on the circumstances of use. Many bonding media have been used over a wide range of temperatures and moisture contents. Silicone resins, wax, mineral greases, and glycerine are commonly used at room temperature. Alcohols can be used at low temperatures. Methods of creating the bond vary with the testing conditions (the nature of the method used for velocity or attenuation measurements, the temperature, the hardness of the wood sample, etc.). With hard woods, when the specimen is large enough, the transducer may be sometimes screwed into the sample and no coupling medium is needed.

Because the aim of our analysis is to report the way in which accurate ultrasonic measurements can be taken, it is evident that the coupling losses must be as small as possible at all frequencies. In any case the losses due to the transducer bond and to the system can be reasonably well measured by the method described in the previous sections of this chapter.

Table 4.11. Influence of coupling media on velocity V_{TT} of propagation of longitudinal waves in *Pinus* spp. at 12% moisture content. (Bucur 1984a)

Coupling media	Velocity (m/s)	Notes
No coupling	1,000	Transducers applied to the specimen under low pressure
Cellophane sheets		
0.03 mm	1,029	If surface of the specimen is clean, the reading is easy to perform; during experiment integrity of sheets must be verified
0.02 mm	973	
Mineral grease	1,004	Grease could penetrate specimen, easy handling
Medical gel	1,004	No penetration of specimen, easy handling
Gel SWC Panametrics	1,050	Very good bond, very absorbent by wood

Table 4.12. Effects of penetration of coupling materials in wood on velocity measured in sitka spruce. (Kamioka and Kataoka 1982, with permission)

Material	Difference (%) in velocity in L, R, and T directions					
	Coupling material effect			Penetration effect		
	L	R	T	L	R	T
Vaseline	3.08	3.98	3.96	3.24	0.54	1.41
Grease	5.99	4.21	4.79	1.49	2.49	1.05
Machine oil	4.95	4.94	4.10	2.62	1.59	1.69
Water	5.20	2.81	4.81	2.47[a]	13.66[a]	13.29[a]

[a] Specimens immersed in water. The reference value is considered for measurements on specimens in direct contact with the transducer. (For small, clear specimens this reference must be considered with care.) (Data from Kamioka and Kataoka 1982)

The effects of the thickness of the coupling medium can be neglected if a very thin coating couplant is used. For precise measurements, a well-defined pressure applied to the specimen through the transducer is required for reproducible measurements of attenuation. Force transducers or strain gauges can be installed on the transducer holders to measure the applied pressure to the specimen. Great care is required with specimens of low density (e.g., balsa) because the applied pressure can affect the measured velocity and attenuation, particularly high frequency, or even break the fragile specimen. Table 4.11 reports observations concerning the influence of various types of coupling media on the ultrasonic velocity measurements.

In practice, the changes induced by the penetration of the coupling media into the wood specimen can produce unexpected experimental errors (Table 4.12). The error initially encountered is the apparent unstable velocity and attenuation measurements. Our understanding of these results is that the wood specimen absorbs the coupling medium to a significant degree, the characteristic acoustic impedance is changed, and the transmit–receive response is modified. To avoid such situations, the thin layer of coupling medium on the transducer surface can be covered with a cellophane sheet (transparent wrapping material made from viscose). (Also, note that the acoustic impedance of cellophane matches well that

of wood.) This protective layer keeps the surface of the wood clean and the results are reliable.

Progress in ultrasonic transducers used in the direct contact procedure has been achieved using a dry coupling layer or noncontact transducers, using the air as the coupling medium.

When the immersion technique is used, particular care is necessary to maintain the moisture content of the specimen. One of the best methods is to envelop the specimen in a surgical membrane that preserves the sample from the penetration of external humidity.

4.3.2.3 Specimens of Finite Dimensions

Specimens of finite length and width can affect the conditions of the propagation of ultrasonic waves in an infinite medium. It is usually desirable to have the diameter of the sample several times greater than the diameter of the transducer (especially at low frequencies with highly divergent beam) in order to reduce side wall effects. However, larger-diameter transducers are more difficult to bond well to the sample. If the transducer fully covers the end of the sample, the transmission phenomenon confines the wave to the specimen (cylindrical rod or slab, etc.) as in a wave guide.

Principally this section analyzes the influence of the finite size of specimens on ultrasonic longitudinal wave velocity measurements. To complete the discussion two cases are presented, namely specimens of constant length and of variable cross section, and specimens of constant cross section and variable length.

Spruce specimens of constant length (300 mm) and of initial cross section of 120×100 mm were repeatedly planed to modify the ratio of width to thickness from 1 to 14. For every value of this ratio the longitudinal wave velocities V_{LL}, V_{RR}, and V_{TT} were measured (Fig. 4.20). The velocity V_{LL} is strongly and continuously affected by the ratio b/h. The maximum velocity V_{LL} is obtained when the ratio b/h lies between 1 and 2 and the specimen is a rod and b and h are greater than the wavelength. In this case the velocity of a longitudinal plane wave was probably measured. The minimum V_{LL} was measured for the ratio b/h=13–14, when the specimen was a plate and h was smaller than the wavelength. The measured velocity corresponds to plate wave velocity (S_0 mode). The values of the velocities V_{RR} and V_{TT}, corresponding to the measurements on the transverse section of the specimen, are less affected by the modification of the geometry of the section. It seems that for the ratio b/h=10 or higher, there is no influence of the cross section on V_{RR} and V_{TT}. We note that the dimensions of the specimen corresponding to the propagation in R and T directions are greater than 2λ. For this reason the velocities V_{RR} and V_{TT} are not influenced by the modification of the size of the specimen.

Figure 4.21 shows the measurements on beech specimens with constant cross section and variable length. Specimens of 600 mm initial length and cross section of 10×10, 20×20, 30×30, and 40×40 mm were shortened successively from initial length to 25 mm. The longitudinal velocity V_{LL} is nearly constant when the ratio of length to width is varied from 20 to 40. Below this limit V_{LL} diminishes. From the same figure it can also be deduce that there is no influence of the length on V_{LL}. The velocity in dry conditions (12% moisture content) is always higher than the velocity in green conditions.

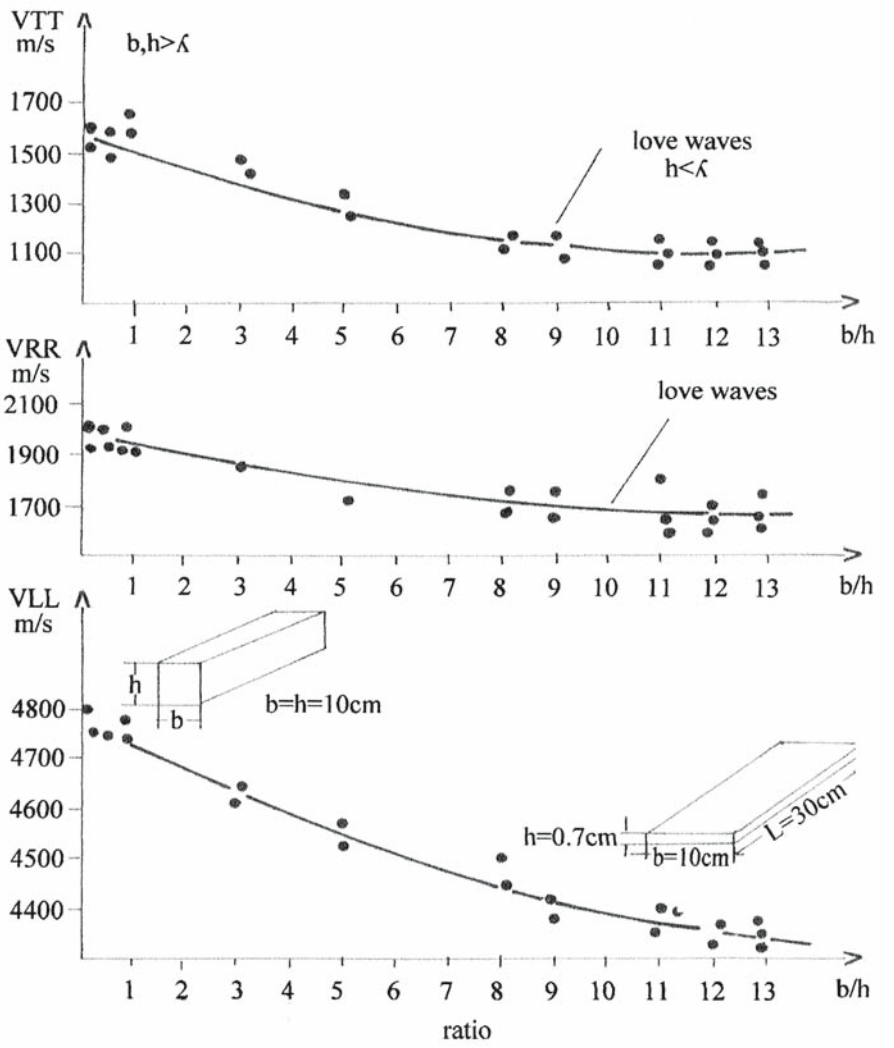

Fig. 4.20. Influence of specimen cross section on velocities measured in spruce, when length of specimen is constant. Dimensions of the specimens at begining of experiment were L=30 cm, b=10 cm, and h=10 cm. At end of experiment, L=30 cm, b=10 cm, and h=0.7 cm. For experimental reasons, the corresponding anisotropic axes were selected as follows: axis L following the length (*L*) of the specimen; axis R following the width (*b*) of the specimen; axis T following the thickness (*h*) of the specimen. (Bucur 1984a)

The influence of path length on the velocity V_{LL} when the specimen is simultaneously shortened and planed in cross section is shown in Table 4.13. The V_{LL} diminishes by about 12% between the shorter and the longer length. This fact is connected with the reduction of the dimensions of the transverse section and can be explained by mode conversion phenomena (from bulk longitudinal waves in an infinite solid to longitudinal waves in a rod).

Another interesting aspect is to study the influence of the geometrical shape of the specimen on velocity values. Table 4.14 gives the values for horse chest-

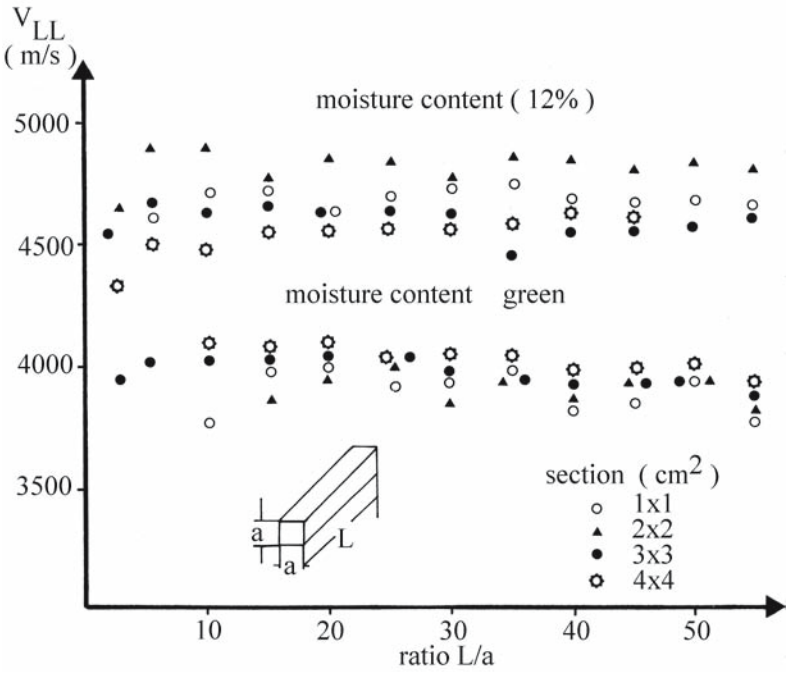

Fig. 4.21. Influence of length of specimen on V_{LL}, when the cross section is constant . Measurements on beech when green and at 12% moisture content. (Bucur 1984a)

Table 4.13. Influence of path length on ultrasonic velocity V_{LL} measured in parallelepiped spruce specimens at 12% moisture content at 1 MHz using broadband transducers. (Bucur 1984a)

Specimen type	Specimen dimensions (mm)			Ratio	V_{LL}
	Length (l)	Width (b)	Height (h)	(lb)	(m/s)
Infinite solid	180	60	60	3	5,570
Infinite solid	120	40	40	3	5,100
Rod	60	20	20	3	4,900

Table 4.14. Influence of path length on ultrasonic velocities in horse-chestnut wood at 12% moisture content. Tone burst technique at 1.5 MHz with 12.5-mm-diameter transducers using the transmission technique. (Bucur and Perrin 1988a, with permission)

	Characteristics of the specimen							
	Size (mm)			Section	Ratio	Velocity (m/s)		
	L	R	T		R/T	V_{LL}	V_{RR}	V_{TT}
Cylinder	160	18	18	Circle	1	5,298	1,521	1,269
Parallelepiped	70	70	22	Rectangle	3	4,975	1,532	1,263
Disk	35	35	22	Square	1.6	5,013	1,562	1,261

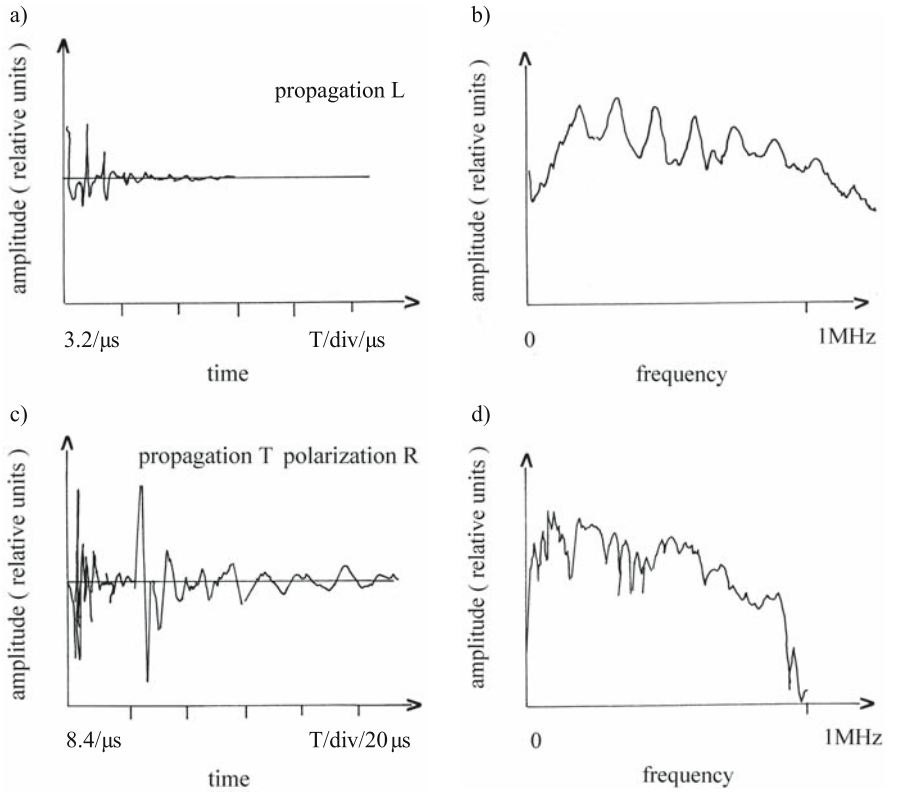

Fig. 4.22. Pulse excitation with longitudinal waves (**a**, **b**) and transverse waves (**c**, **d**) on a poplar cubic specimen in time and frequency domains. (Böhnke and Guyonnet 1991, with permission)

nut for the longitudinal velocity V_{LL} and for transverse velocities V_{LR} and V_{LT} on cylindrical specimens and on disks. From this experimental situation it can be deduced that the values of velocities are not affected by the geometry of the specimen.

The multiplicity of modes propagating in wood can be seen in Fig. 4.22 in which the typical behavior of cubic poplar wood specimens in the time domain and frequency domain are presented. From the frequency spectrum of longitudinal waves we can see the lobe patterns corresponding to the geometry of the specimen as well as the peaks made by the vibration of fibers of 2–3 mm length in the region corresponding to frequency higher than 1.6 MHz. From the frequency spectrum of shear waves the annual ring width and the proportion of latewood in the annual ring can be deduced. The complexity of modes propagating in wood can also be seen in Fig. 4.23, when a disk-type specimen is excited at 45° with shear waves in four symmetric points. From this figure we can note the following:

- The main amplitude of the signal corresponds to the arrival of the quasi-transverse wave. This component is conserved and arrives at the same time for all excitation positions. There is no interference between the wavelength and the anatomical elements.
- The smaller amplitude of the signal corresponds to the arrival of the quasi-longitudinal wave. This component shows a displacement of Δt. The wavelength

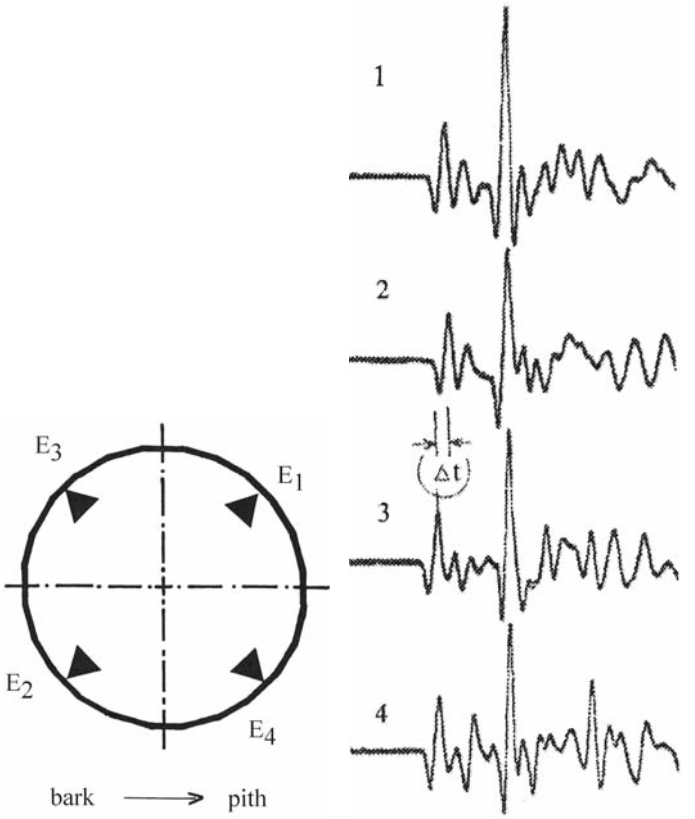

Fig. 4.23. Mode conversion phenomena induced on a specimen excited at 45° with transverse waves. *1*, *2*, *3*, and *4* Signals corresponding to excitation points E_1, E_2, E_3, and E_4. The *peak* corresponding to the maximum of amplitude is related to the quasi-transverse wave. Position of this peak is conserved for different points of excitation. The *second peak* in amplitude corresponds to the quasi-longitudinal wave and is affected by anatomical structure. This peak shows a Δt displacement. (Bucur and Perrin 1988, with permission)

is comparable with the fiber length. We suppose that the time difference illustrates the misalignment of fibers.

In the future, more elaborate techniques, such as ultrasonic spectroscopy (Gerike 1970; Fitting and Adler 1981; Alippi 1989, 1992) and signal processing as high resolution spectral analysis (Chen 1988), and evaluation in the time-frequency domain by means of the Wigner-Ville distribution (Flandrin 1988), could improve the understanding of phenomena related to ultrasonic wave propagation in wood microstructure.

4.3.2.4 Influence of the Physical Properties of Wood on Measurement of Ultrasonic Velocity

The physical properties of wood on which our attention is focused in this chapter are: the density, a parameter that characterizes each species; the moisture con-

Table 4.15. Ultrasonic velocity in earlywood and latewood and density components in X-ray microdensitometric analysis of resonance in spruce. Measurements were made on very thin (3×3 mm^2) radiographic specimens. This fact induces dispersion of ultrasonic waves and could partially explain the relatively small values measured in earlywood and latewood when compared to solid wood. (Bucur 1983b)

Parameters	Earlywood 74% annual ring	Latewood 26% annual ring	Solid wood 100% annual ring
V_{LL} (m/s)	3,226	3,650	5,500
V_{TT} (m/s)	1,062	1,468	1,500
ρ=X-ray density (kg/m^3)	364	636	426
Correlation coefficients between V and ρ	0.578**	0.613**	–

tent when wood is in the green condition or in the air-dried condition; and the structure of the annual rings, with the corresponding proportions of earlywood and latewood.

The experimental relationship between density (ranging from 200 to 900 kg/m^3) and sound velocity (2,500–5,800 m/s) in more than 40 species of softwoods and hardwoods, deduced from the resonance frequency method by Barducci and Pasqualini (1948), is statistically significant at 5%. This means that the empirical relationship between these parameters is not very strong. Generally speaking, small values of velocity V_{LL} correspond to high densities. This seems natural if we consider the anisotropic nature of wood as well as its structural organization. For this purpose Burmester (1965) produced a more refined analysis in which he plotted separately the ultrasonic velocity and density of two species, spruce and limba. Burmester found that spruce reacts with ultrasonic waves as a complicated natural composite material, whereas limba behaves more like a homogeneous orthotropic solid.

Let us now analyse the influence of earlywood and latewood from the annual ring on ultrasonic velocity. The opinions of different authors are rather divergent. Burmester (1965) agrees that the velocity in isolated earlywood is slower than that measured in solid wood. Yiannos and Taylor (1967) reported higher velocities in latewood than in earlywood in pine. Gerhards (1978) found that earlywood or latewood had no effect on stress wave velocity measurements parallel to the grain in sitka spruce and southern pine. The data reported are strictly related to his experimental procedure, in which he used accelerometers clamped onto earlywood or latewood on transverse sections of specimens. It is surmised that the probe was not small enough and the two overlapped.

Technological progress in ultrasonic transducers in last 10 years has allowed fine measurements to be made, related to a contact surface of less than 1 mm^2. Measurements on spruce in the 1-MHz frequency range (Table 4.15) with longitudinal waves in L and T directions are related to the density determined by an X-ray technique. Ultrasonic measurements were performed on the specimens required for microdensitometric analysis (3×3 mm^2 section). The values of longitudinal velocities in L and T directions, V_{LL} and V_{TT}, are different in earlywood and latewood and smaller than those measured in solid wood, probably because of the dispersion induced by the geometry of the thin specimen. The velocities V_{LL} and V_{TT} in latewood are slightly higher than in earlywood.

Relationships statistically significant at 1% have been established between velocities and corresponding density of earlywood. Prior data are primarily inter-

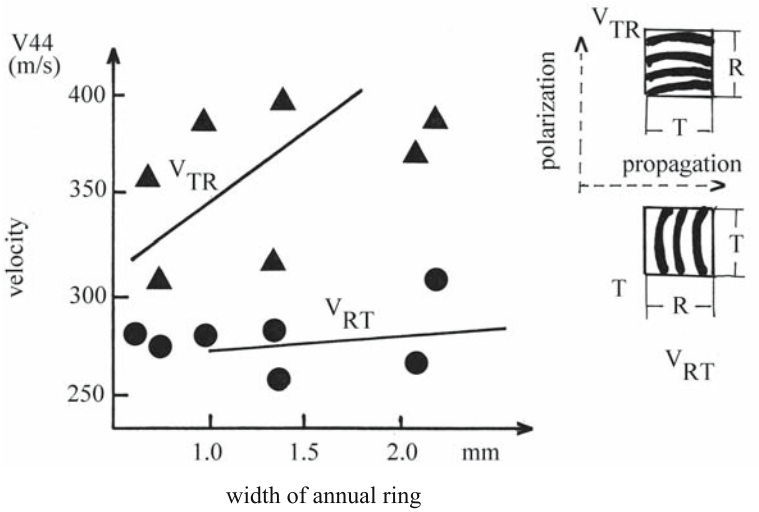

Fig. 4.24. Discrepancy in transverse velocities V_{RT} and V_{TR} due to birefringency and to the waveguide effect in spruce. Note influence of annual ring width on V_{TR} where the propagation vector is parallel to the layering (T). There is no influence on V_{RT} where the propagation vector is parallel to R. (Bucur and Perrin 1988, with permission)

esting methodologically; nevertheless they can be used as reference for producing composites for the musical instrument industry.

The influence of the curvature of rings is a pertinent question in relation to the correct measurement of V_{RR}, when bulk compressional waves propagate in the R direction, perpendicular to the annual ring. As regards this case, Woodhouse (1986) emphasized the sample-size constraint and pointed out that the continuum theory employed in ultrasonic characterization using an orthotropic model ignores this curvature. To clarify this point several experiments have been performed by Bucur and Perrin (1987). The effect of the curvature of rings on V_{RR} was studied on two disks cut in the RT plane. The first was 10 cm in diameter representing a cross section of a young spruce tree on which V_{RR} was 1,574 m/s. The second disk was cut from the first and was 4 cm in diameter. On the second disk the relative curvature was greater but the velocity was the same, V_{RR}=1,579 m/s. Similarity of the values enables us to conclude that for the direct transmission technique, when longitudinal bulk waves of 1 MHz are used, the curvature of rings has no influence on V_{RR}. The situation may be different for transverse waves (Fig. 4.24).

Using the acousto-ultrasonic technique, Lemaster and Quarles (1990) analyzed the influence of the layered structure on a parameter related to the amplitude and energy of the ultrasonic signal [measured in root mean square (rms) voltage], induced by both the alternation of earlywood and latewood and that of the radius of curvature of the annual ring. When a direct transmission technique is employed, which probably leads to the propagation of a bulk longitudinal wave in the radial direction of the specimen, the curvature of the rings has no effect on the rms voltage. When "side excitation" was used, the measured rms signal (probably corresponding to a surface wave propagating in the LT plane) for pine for the concave interface was 1.2 V and was greater than that for the convex interface (0.75 V). The high amplitude of the signal observed in this case could be

explained by the fact that for the concave situation the signal travels from earlywood to latewood and the acoustic impedance of layers increases gradually. A similar situation could be observed for shear waves when V_{TR} was measured.

It is well known that to define the C_{44} term of the stiffness matrix, the shear velocity V_{TR} or V_{RT} or both are measured. (Note that the first index is related to the propagation direction and the second index is related to the polarization direction.) Modulation of the transverse waves by the structure is strongly related to the propagation and polarization directions and birefringence phenomenon is observed. Data are given in Fig. 4.24. It can be seen that V_{RT} is not affected by the ring curvature, since the direction of propagation is R.

The opposite effect is observed on V_{TR} in species with a pronounced difference between latewood and earlywood. This velocity is probably related to the guide wave effect induced by the latewood with thick walls and high density. For softwoods (spruce, Douglas fir) the difference between V_{TR} and V_{RT} is in the order of 10–15% and the figure for ring porous oak is 17%. In diffuse porous hardwoods the discrepancy between the two values is only 5%. Further investigation of these effects requires that the waveguide effects and dispersive propagation due to the interaction of ultrasonic waves with the microstructure be related to the frequency and to the wavelength (Fig. 4.25).

Evidence of the stop bands effect induced by the presence of layered annual ring structure was demonstrated by Feeney et al. (1998), using the model developed by Brillouin and Prodi (1956) and James et al. (1995) which stated that a "finite number of layers, as little as five, can give rise to the existence of sonic band gaps". Feeney et al. (1998) used the immersion technique, scanning the wood sample in L direction, with a 0.5-mm hydrophone with a focused transducer of 2 MHz, and clearly demonstrated that the pattern of velocity variation corresponds to the densitometric variations observed in annul rings. Velocities higher than 4,000 m/s were measured for latewood. For earlywood the velocities were in the range of 2,600–3,000 m/s. The presence of juvenile wood in spruce "gives rise to more potential stop bands than the mature wood" and "the sharp impedance step between earlywood and latewood provides a strong potential scattering source within the material along the radial axis". "Even frequencies as low as 100 kHz give rise to wavelength of a similar order of magnitude as juvenile ring widths" (about 5 mm).

The influence of frequency on ultrasonic velocities was studied with the sinusoidal burst direct transmission technique as described by Bucur and Feeney (1992). The frequencies were 100, 250, 500, 1,000, and 1,500 kHz. Both longitudinal and transverse waves were used. A pulse length of four cycles was employed, thus producing a narrow band ultrasonic wave at driven frequency. The following observations can be made from Fig. 4.25a: $V_{11}=V_{LL}$ is strongly influenced by frequency, with a large increase in velocity from 100 to 250 kHz and a steady, but smaller, increase in velocity from 250 to 1.5 MHz. The relatively small value of velocity measured at 100 kHz was probably induced by geometric dispersion. $V_{22}=V_{RR}$, $V_{33}=V_{TT}$, $V_{44}=V_{TR}$, $V_{55}=V_{LT}$, and $V_{66}=V_{LR}$ are insensitive to the frequency variation for frequencies higher than 250 kHz.

Up to this point it has been assumed that the wavelength is much longer than the material structural dimensions. However, as soon as the wavelength matches the dimensions of layers or of cells, the velocity is dependent on frequency.

The choice of the most interesting frequency field of investigation must be related to a wavelength that is comparable with the dimensions of anatomical elements, which vibrate as elementary resonators. Only the frequency compo-

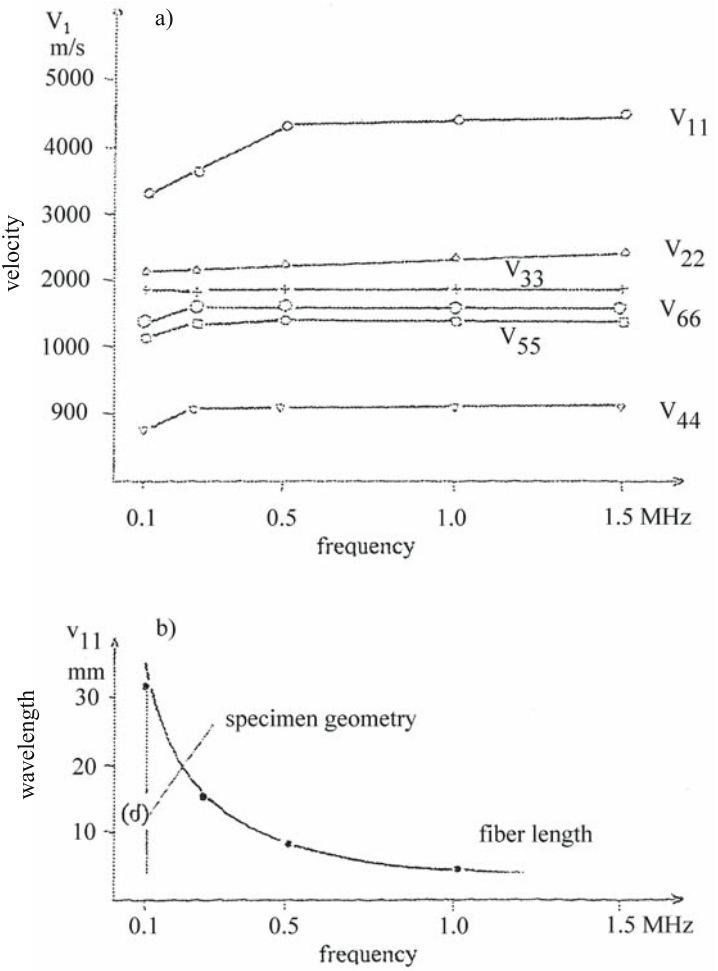

Fig. 4.25. Influence of frequency on ultrasonic velocity measurements. **a** Velocities versus frequency from 0.1–1.5 MHz; **b** wavelength corresponding to V_{LL} versus frequency. Specimen geometry is seen at 0.1 MHz and fiber length at 1–1.5 MHz. *d* Dimension (size of the specimen) determining its geometry. (Bucur 1984a)

nent that matches the natural frequency of those resonators (Fig. 4.25b – the fibers vibrate in the range 1–1.5 MHz) can give a detailed answer to the ultrasonic wave–wood structure interaction, and can, at the same time, explain the overall wood acoustic properties.

The microstructure–wavelength interaction in the solid wood that behaves like a filter with alternate pass bands and stop bands using ultrasonic spectroscopy is an interesting research aspect for the future.

4.4 Attenuation of Ultrasonic Waves in Wood

The basis of the ultrasonic evaluation of the viscoelastic behavior of wood is associated with measurements of attenuation coefficients. Pioneering work on poly-

crystalline media (Papadakis 1965, 1967, 1968, 1990) and on biological tissues, polymers, and inhomogeneous media in general (Chivers 1973, 1991) has shown that attenuation is a valuable parameter which may give information about the structure and the environmentally influenced conditions of the polycrystalline and biological materials through which the ultrasonic waves are propagated. The parameters of ultrasonic wave propagating in solid structure can be influenced by a broad range of factors, such as the physical properties of the substrate, the geometrical characteristics of the specimen under test (macrostructural and microstructural features), the environmental conditions (temperature, moisture content, mechanical loading), and the measurement conditions (sensitivity and frequency response of the transducers, their size and location, the coupling medium, and the dynamic characteristics of the electronic equipment).

The numerical significance of attenuation depends on the specific measurement conditions (Bucur and Feeney 1992). For wood material, values of attenuation coefficients have been reported by Bucur and Ghelmeziu (1977), Okyere and Cousin (1980) (α_L=5 dB/10^{-2} m; α_R=22 dB/10^{-2} m for red pine at 1 MHz and 48% moisture content), and by Böhnke (1993) (for dry sugi wood and longitudinal waves: α_L=2.1 dB/10^{-2} m and α_R=4.7 dB/10^{-2} m; and for shear waves: α_{LR}=3.4 dB/10^{-2} m and α_{RL}=14.3 dB/10^{-2} m).

4.4.1 Theoretical Considerations

Up till now, we have assumed that wood is a viscoelastic linear solid, having an orthotropic symmetry. Therefore, we will consider the effective properties of an equivalent solid medium.

The scattering of an ultrasonic wave in this medium results in frequency-dependent wave velocity and attenuation. The dispersion equation (Christensen 1971, 1979; Hosten et al. 1987; Chevalier 1988, 1989; Hosten 1991) relating all the parameters of propagation phenomena in anisotropic solids (when the terms of the Christoffel tensor [Γ_{ij}*] and stiffness tensor are complex, notably [C_{ij}*], and also k is complex, $k^*=k\text{-}i\alpha$ and $V=\omega/k^*$) is as follows:

$$[\Gamma_{ij}^{*}(\omega) - \Lambda^{*} \cdot \delta_{ij}] = 0 \tag{4.63}$$

where ω is the frequency and δ_{ij} is the Kroneker tensor.

For in axis propagation, the dispersion equation takes the form:

$$\begin{bmatrix} \Gamma_{11} - \Lambda^{*} & 0 & 0 \\ 0 & \Gamma_{22}^{*} - \Lambda^{*} & 0 \\ 0 & 0 & \Gamma_{33}^{*} - \Lambda^{*} \end{bmatrix} = 0 \tag{4.64}$$

The eigenvalue Λ^* of the dispersion equation (Chevalier 1989) is:

$$\Lambda^{*} = \frac{\rho V^2}{\left(1 - \frac{i\, a \cdot V}{\omega}\right)^2} \tag{4.65}$$

where ρV^2 is the real part of the diagonal stiffness tensor and $\frac{i\alpha V}{\omega}$

is the ratio of the imaginary to the real part of the stiffness terms.

If $\alpha<1, \frac{i\alpha \cdot V}{\omega} < 1$, the eigenvalue can be written as $\Lambda^* = \rho V^2(1 + 2i\alpha \cdot V/\omega)$,

where $2\alpha \times V/\omega$ is the ratio of the imaginary and real part of the stiffnesses.

4.4.2 Measurement Technique

Attenuation measurement can be performed either with broadband pulses (containing a wide range of frequencies) using ultrasonic spectroscopy, or with narrow band pulses using burst excitation at a fixed frequency (Bucur and Böhnke 1994). Both cases are analyzed below.

The calculation relationship adopted for attenuation coefficients is:

$$\alpha_{ij} = \frac{1}{d} \ln \frac{A}{A_0}$$

4.4.3 Factors Affecting Attenuation Measurements in Wood

The propagation of ultrasonic waves in wood may be attenuated by three main factors: the geometry of the radiation field, scattering, and absorption. The first factor is related to both the properties of the radiation field of the transducer used for measurements (beam divergence and diffraction) and wave reflection and refraction occurring at macroscopic boundaries of the medium. These factors are related to the geometry of the specimen. Scattering and absorption are phenomena related to the material characteristics.

4.4.3.1 Geometry of the Specimen

To study the influence of the geometry of specimens on ultrasonic attenuation, cylindrical samples of the same diameter and of different length were selected. Figure 4.26 shows attenuation expressed as amplitudes versus frequency for cylindrical specimens of beech (diameter: 20×10^{-3} m; length: 50, 100, 135, and 200×10^{-3} m). For small specimens the attenuation decreased linearly with the frequency in the range 1–2 MHz. For long specimens, the central frequency moved to the lower frequency and no linearity was observed.

Both cut-off frequency and frequency for which there is an amplitude maximum depend on the insonified volume of specimen, which of course increases with the length of the sample. The wave guide effect is more evident for the specimen having small diameter.

For the specimen of length 50 mm, excited in the L direction, the cut-off frequency is about 2 MHz, for a 135-mm-length specimen the cut-off frequency is about 1.35 MHz. For long specimens the frequencies are shifted to the lower ranges, which means that the attenuation is greater in long specimens than in short specimens. Thus, the proposed linear viscoelastic model seems to be quite satisfactory. It is possible then that a recommendation could be made that relatively small specimens (20–50 mm length) be selected for laboratory measurements. In such a case it is vital to verify that the propagation phenomena take place in the

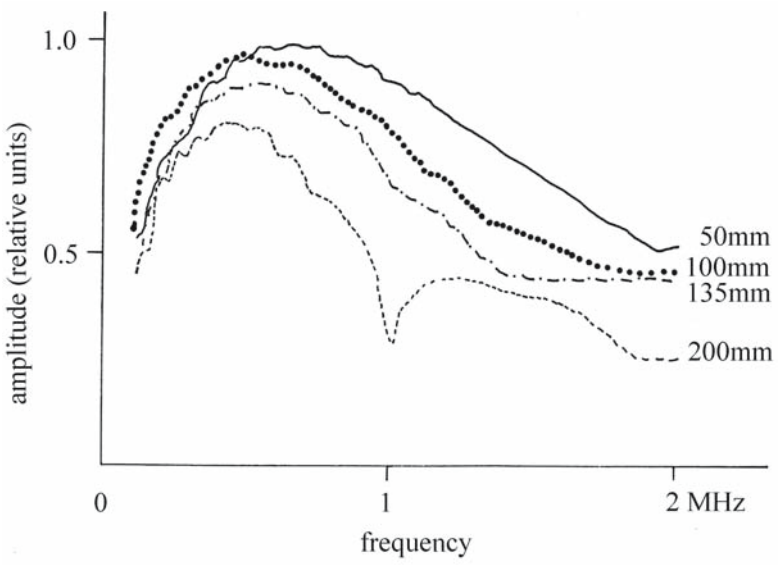

Fig. 4.26. Attenuation (expressed as amplitude) versus frequency for cylindrical specimens of beech. (Bucur and Böhnke 1994, with permission)

far field and no resonance occurs. For this reason the wavelength λ and the near field length were calculated (Table 4.16) when measurements were performed on short specimens, cubes, and cylinders of 20×10^{-3} m length. The reader should note that the dimensions of the cubic specimens are greater than the wavelength, in all anisotropic directions. The near field of radiation in the longitudinal direction is between 1.8 and 5.5 mm; in the radial direction it is between 3.3 and 11 mm; in the tangential direction it is between 4.5 and 16.3 mm. Short cylindrical specimens must therefore be avoided.

As the microstructure of a solid governs its mechanical properties, it seems natural to consider that the mechanisms of wave attenuation should be related to the characteristics of the individual grain of the microstructure (the cell in the case of wood). Moreover it is interesting to compare now the wavelength with some data related to dimensions of wood anatomical elements. It is well known (Panshin and de Zeeuw 1980) that the length of wood cells (tracheids) in conifer species is about 3–4 mm and in broadleaved species the length of the fibers is about 1 mm. The dimension of cells in the T direction for spruce is about 30 μm. In the radial direction this dimension may be 50 μm. The proportion of medullary rays is about 7% of the total volume.

Broadleaved species are very different and it is difficult to provide figures for general characteristics. For this reason we have selected maple (*Acer* spp.) as an example. In *Acer* spp. the percentages of the different elements of the total volume of wood are 18% vessels, 65% fibers, and 15% rays. The fiber length is about 1 mm and the vessel length is about 0.5 mm. The diameter of the vessels is about 300 μm. The fiber diameter is about 30 μm.

Coming back to the links between the wavelength and the dimensions of the anatomical elements, it is to be noted that in cubic specimens, insonified with longitudinal waves, in the longitudinal direction, the wavelength and the cell length are both on the scale of millimeters. Probably the propagation takes place

Table 4.16. Length of radiation field, wavelength, and attenuation measurements expressed by signal amplitude at a given frequency in beech. (Böhnke 1993)

Anisotropic direction	Velocity (m/s)	Attenuation (dB)	Frequency (kHz)	Wavelength λ (mm)	Φ2/4λ (mm)
Cylinder 20 mm long, transducers 1 MHz, Φ=14 mm					
L	4,887	17	151	32	1.5
R	2,492	12	79	32	1.5
T	1,735	14	75	23	2.0
Cube 20-mm size, transducers 1 MHz, Φ=14 mm					
L	5,609	24	705	9	5.5
R	2,648	35	635	4	11.0
T	1,772	48	584	3	16.3
Cylinder 20 mm long, transducers 5 MHz, Φ=7 mm					
L	4,734	16	195	24	0.5
R	2,151	13	254	9	1.5
T	1,576	13	159	8	1.5
Cube 20 mm size, transducers 5 MHz, Φ=7 mm					
L	4,305	27	608	7	1.8
R	2,196	40	591	4	3.3
T	1,609	57	217	7	4.5

in the stochastic scattering regime. In the radial and tangential directions the wavelengths significantly exceed the mean cell dimensions (i.e., in the R direction λ=4 mm and the cell dimension may be 50 μm; in the T direction λ=3 mm and the cell dimension may be 30 μm). In this case, probably the propagation takes place within the Rayleigh scattering regime.

4.4.3.2 Characteristics of the Material

The influence of the characteristics of the material on scattering is analyzed in three typical situations: when wood is compared with an isotropic solid, when different anisotropic axes are compared in the same species, and when the same anisotropic axis is considered in different species.

When wood material is compared with an isotropic solid we need to analyze the amplitude spectrum (Fig. 4.27), in which we note for wood the shift in central frequency with respect to the low frequency region. The influence of the different material anisotropic directions on attenuation is shown in Fig. 4.28a, in which the signal in the time domain is shown for L, R, and T directions. It should be noted that for the same beech cubic specimen, the more dispersive the direction of propagation, the more the signal looses high frequency components and consequently becomes wider. In the frequency domain (Fig. 4.28b) we analyze the amplitude spectra corresponding to the L and T directions, insonified with longitudinal waves. In the spectrum corresponding to the L direction the structural vibration is between 600 and 700 kHz. From this spectrum, if the value of the phase velocity is known (i.e., 4,000 m/s) it is possible to determine the fiber

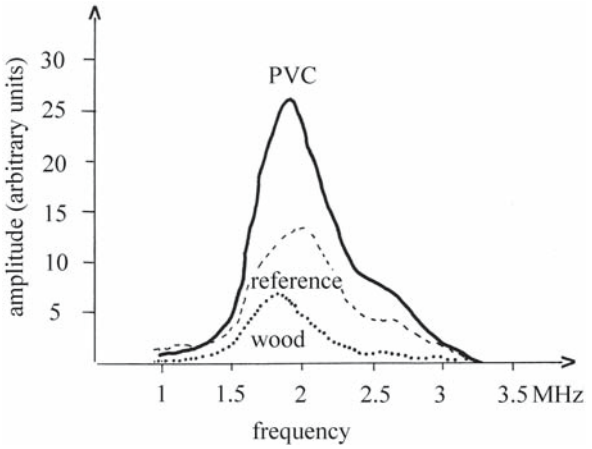

Fig. 4.27. Amplitude spectra of spruce and polyvinylchloride (*PVC*) with broadband transducers. (Bucur and Böhnke 1994, with permission)

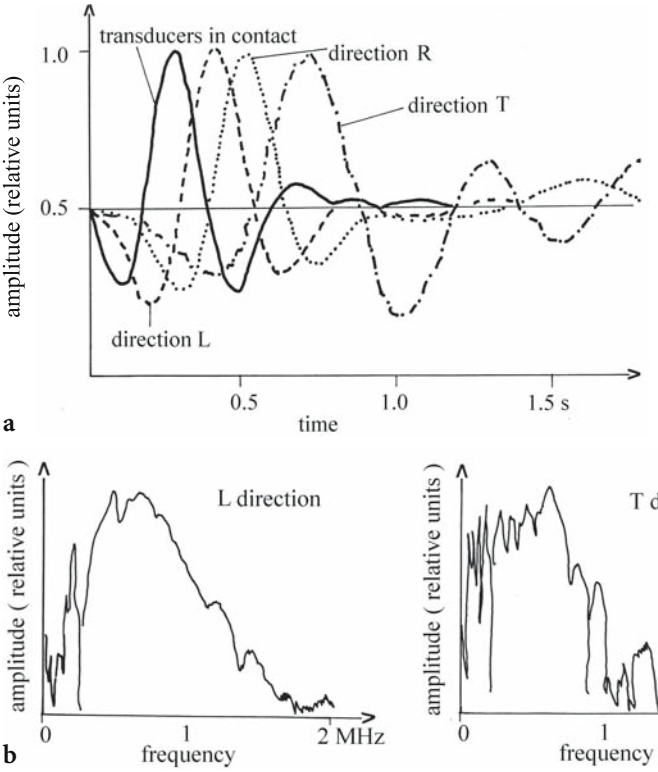

Fig. 4.28. Amplitude in different anisotropic directions measured with the same cubic specimen of 20 mm size. **a** In the time domain for propagation in L, R, and T directions, using broadband transducers of 1 MHz central frequency and longitudinal waves. **b** In the frequency domain for propagation in L and T directions, using broadband transducers of 5 MHz central frequency and longitudinal waves. (Böhnke 1993, with permission)

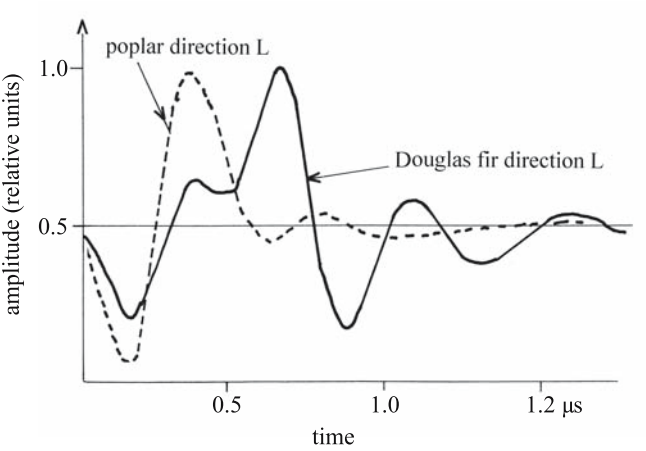

Fig. 4.29. Propagation of ultrasonic waves in longitudinal direction in a cubic specimen of poplar and Douglas fir. (Bucur and Böhnke 1994, with permission)

length (approximately 5 mm), but for this purpose the appropriate methodology for phase velocity measurements must first be developed.

In the T direction the spectrum is very complex and is similar to the spectrum obtained for periodic layered composites (Scott and Gordon 1977). The periodicity observed in the specimen is induced by the annual rings, and coincides with the periodicity of the highest amplitude peaks in the spectrum.

When we compare the same anisotropic direction L (Fig. 4.29) in different species (Douglas fir and poplar), we note that the broader signal is observed in the most heterogeneous species (Douglas fir). This behavior could be associated with the anatomical scatter in the structure. The richer the structure is in scatterers of various densities, the more important the dispersion phenomena are, as can be seen in the case of Douglas fir.

Table 4.17 shows the attenuation coefficients for all the anisotropic axes and planes calculated for excitation by both longitudinal and shear waves. It can be seen that:

- The attenuation coefficients increase with frequency for both longitudinal and transverse waves.
- For longitudinal waves, the T direction exhibits the highest attenuation.
- For transverse waves, generally, there were no significant differences between the attenuation coefficients of waves propagating in different directions.
- The attenuation coefficients of the longitudinal wave in L and R directions are higher in spruce than in maple. This is probably due to important differences in densities in annual ring zones (i.e., in spruce in earlywood the density is 300 kg/m^3 and in latewood the density is 900 kg/m^3). In spruce the proportion of the latewood is 15–20% of the annual ring width. In maple the latewood zone is very narrow, about 5%.

The propagation phenomena on the scale of the structure of ultrasonic waves in wood can be understood using a simplified acoustical model (Bucur 1980b). Wood cells may be treated as "tubes" of cellulosic crystalline substance embedded in an amorphous matrix – lignin. Solid wood is then a rectangular array of tubes embedded in a matrix. The longitudinal orientation of the tubes is slightly

Table 4.17. Attenuation coefficients $\alpha_{ij=}-1/d \ln P/Po$ (in Nepers/cm) and velocities (in m/s) in curly maple and common spruce, measured with the sinusoidal burst transmission technique and longitudinal and transverse waves. 1 dB/10^{-2} m=8.69 Np/10^{-2} m. (Bucur and Böhnke 1994, with permission)

Parameters	Frequency (MHz) 0.10	0.25	0.50	1.0	1.5
Curly maple					
Longitudinal waves					
α_{11}	1.55	1.62	1.62	1.75	1.90
V_{11}	4,332	4,409	4,540	4,706	4,559
α_{22}	2.30	2.25	2.29	2.47	2.63
V_{22}	2,285	2,270	2,279	2,325	2,340
α_{33}	2.82	2.82	3.03	3.22	3.22
V_{33}	1,254	1,291	1,321	1,316	1,345
Transverse waves					
α_{44}	1.64	1.85	1.85	2.32	2.47
V_{44}	8,69	966	918	918	–
α_{55}	1.68	1.77	2.10	2.47	2.39
V_{55}	1,214	1,350	1,394	1,428	1,399
α_{66}	1.77	1.94	2.05	2.27	2.34
V_{66}	1,342	1,552	1,566	1,602	1,580
Common spruce					
Longitudinal waves					
α_{11}	2.17	2.07	2.10	2.29	2.47
V_{11}	4,458	4,847	5,343	5,327	5,401
α_{22}	2.83	3.02	3.22	3.22	–
V_{22}	1,612	1,741	1,832	1,832	–
α_{33}	2.71	3.02	3.03	3.02	3.22
V_{33}	1,283	1,400	1,321	1,325	1,346
Transverse waves					
α_{44}	Signal not analyzed				
V_{44}	Signal not analyzed				
α_{55}	1.62	1.62	1.85	2.06	2.17
V_{55}	1,310	1,320	1,356	1,383	1,372
α_{66}	1.64	1.71	1.71	2.17	2.36
V_{66}	1,250	1,372	1,383	1,822	1,839

disturbed by horizontal elements, the medullary rays. In the longitudinal direction the dissipation of acoustical energy takes place at the edges of the tubes. Accordingly, the longitudinal axes which are constructed from long elements provide high values of velocities and relatively small values of attenuation. The highest attenuation is expected in the T direction in which no continuous structural elements exist.

Statistical analysis of the influence of the natural variability of wood material on attenuation expressed by measured amplitude is given in Table 4.18. The coefficient of variation in the longitudinal direction was 19%, which is in the same range as for other mechanical properties of wood.

This section obviously does not cover all aspects of attenuation measurements in wood, but it can be noted that the main factors affecting ultrasonic attenuation measurements in wood are related to the geometry of the radiation field, to wave

Table 4.18. Statistical analysis of the influence of natural variability of spruce wood on attenuation expressed by measured amplitude values. (Böhnke 1993)

Statistical parameters	Density (kg/m^3)	Velocity (m/s)	Amplitude (dB)	Frequency (kHz)
Minimum	345	5,512	22.5	628
Maximum	600	6,694	69.7	980
Average	493	6,209	47.0	854
Coefficient of variation (%)	11	4	19	8

reflection and refraction occurring at the macroscopic boundary of the medium (the edge of the specimen), and to the scattering phenomena. Cubic specimens are appropriate for attenuation measurements. In cubes insonified using longitudinal waves, the wavelength and the wood cell length are on the millimeter scale. In the longitudinal direction the propagation takes place in the stochastic scattering regime whereas in the radial and tangential directions it takes place in the Rayleigh scattering regime because the wavelengths exceed the cell dimensions. The attenuation coefficients increase with frequency for both longitudinal and shear waves. Attenuation is lowest in the longitudinal direction and highest in the tangential direction. The richer the wood structure is in scatterers of various densities, the more important the dispersion phenomena.

4.5 Internal Friction in Wood in the Audible Frequency Range

In the audible frequency range the viscoelastic behavior of wood is associated with the magnitude of the damping coefficients. Theoretical bases for the estimation of damping coefficients in solids are given in many reference books (Cremer and Heckl 1973; Read and Dean 1978; Main 1985; Beltzer 1988). Several parameters are used to describe the internal friction or the absorption of mechanical energy by solids in the audible frequency range. The most common are:

- the mechanical damping, tan δ, defined as the "logarithmic decrement", that is the logarithm of the ratio of two subsequent amplitudes of free vibrations calculated as $2\pi \tan \delta$, where δ is the phase angle;
- the quality factor Q, for steady-state forced vibrations, defined by analogy with the theory of electric circuits, as the ratio of the width (Δf) of the resonance curve at half maximum amplitude or at half power level (or at −3 dB) to the resonance frequency f_r $Q = \frac{\Delta f}{f_r}$.

Very often the experimental results are expressed as Q^{-1}.

The different parameters relevant to internal friction phenomena in solids in the audible frequency range and in the ultrasonic range are related as follows:

$$2\pi \tan \delta = 2\pi \frac{\Delta f}{f_r} = 2\pi Q^{-1} = 2a \frac{V}{f_r} \tag{4.67}$$

where V is the ultrasonic velocity and α is the ultrasonic attenuation. This relationship is valid for materials with tan δ <0.2 (Read and Dean 1978). Measurements of internal friction parameters and of ultrasonic attenuation coefficient

Table 4.19. Internal friction in several species determined in L, R and T directions with longitudinal vibrations. Density of the specimens with main axis in L, R, or T direction. (Ono and Norimoto 1985, with permission)

Species	Density (kg/m^3)			Internal friction (Q^{-1})			Anisotropy		
	L	R	T	L	R	T	L	R	T
Sitka spruce	460	449	454	11.2	23.2	24.4	1	2.10	2.20
Lauan	481	489	478	7.6	19.7	20.3	1	2.59	2.63
Makoré	669	673	670	9.5	28.0	33	1	2.95	3.47
Matoa	795	700	674	9.4	27.3	27.5	1	2.91	2.93
Mizunara	630	654	620	107	25.8	28.9	1	2.41	2.70
Yachidamo	570	548	517	8.8	25.1	26.9	1	2.82	3.03

in various kind of solids (alloys, glass, ceramics) have been reported by Smith (1980).

4.5.1 Typical Values of Damping Coefficients

The most complete list of values of logarithmic decrement in L and R directions for a number of species is that of Haines (1979). Measurements in three anisotropic directions for different modes are scarce, however, because of the difficulties in obtaining corresponding specimens for T direction tests. The measurements using the longitudinal mode reported by Ono and Norimoto (1985) are reproduced in Table 4.19.

It is worth noting that $Q_L^{-1} << Q_R^{-1} < Q_T^{-1}$ and the anisotropy ratio deduced as $\frac{Q_R^{-1}}{Q_L^{-1}}$ is typically between 2.1 and 3.0 and

$\frac{Q_T^{-1}}{Q_L^{-1}}$ is between 2.2 and 3.5. In addition, it may be said that the internal friction is smaller in the fiber direction and higher in the T direction.

The damping mechanism in solid wood is caused by the lignin regions. Cellulosic microfibrils are highly crystalline and consequently they have low damping. The variation of damping with the grain angle was reported by Ono (1983a) and some data are reproduced in Table 4.20. The general equation for the prediction of the internal friction with the grain angle is as follows:

$$Q_\alpha^{-1} = Q_{0^\circ}^{-1} + Q_{90^\circ}^{-1} - [Q_{0^\circ}^{-1} \cdot Q_{90^\circ}^{-1}] \cdot [Q_{0^\circ}^{-1} \cdot \cos^2\alpha + Q_{90^\circ}^{-1} \cdot \sin^2\alpha] \quad (4.68)$$

where α is the grain angle.

4.5.2 Damping Coefficients as Indicators of Microstructural Modifications Induced by Different Factors

This section discusses the influence on the damping coefficients of wood of several factors – temperature, moisture content, chemical treatment, and dynamic loading of the specimen.

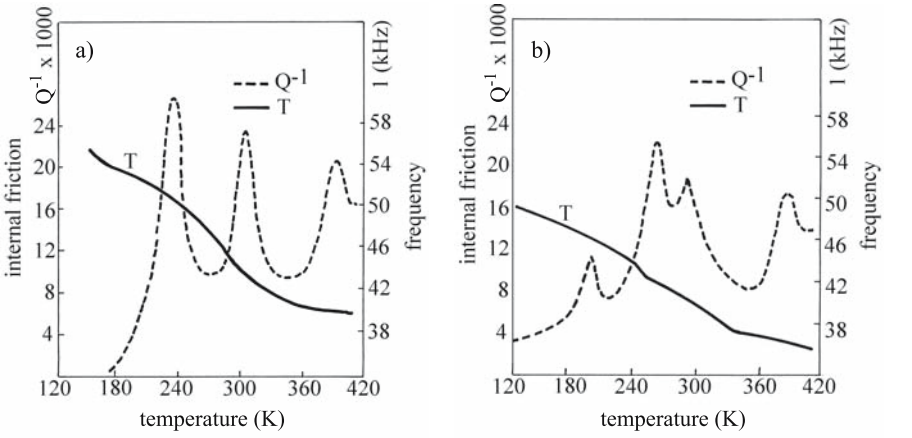

Fig. 4.30. Internal friction and resonance frequency in beech as a function of temperature and moisture content. **a** In longitudinal direction; **b** in radial direction. (Khafagy et al. 1984, with permission)

4.5.2.1 Temperature and Moisture Content

We chose to indicate the way in which the parameter Q^{-1} is able to reflect fine structural modifications in wood induced by an increase in temperature. For this purpose internal friction spectra of beech as a function of temperature are given in Figs. 4.30 and 4.31. In Fig. 4.30 in both anisotropic directions (L and R), two peaks of Q^{-1} were observed associated with corresponding changes in frequencies. At low temperatures, i.e., below 170 K, the molecular motion in amorphous lignin is probably frozen and therefore the frequency variations are very small. The increase in temperature permits dislocations and rearrangement of the structure, probably at the hemicellulose level. This begins at 210 K for specimens in the L direction and at 230 K for specimens in the R direction. A larger damping was observed for acoustic waves that propagate across the fibers (R direction). The increase in temperature softens the amorphous regions, and this is followed by a second transition, occurring in the range 260–300 K and characterized by a broadened peak in L-type specimens. The softening of the material has led to a large decrease in corresponding resonance frequency. With further increase in the temperature (390 K) a third transition is observed, probably corresponding to the glass transition of wood.

The effect of heat treatment on internal friction in woods used for musical instruments has also been reported by Nakao et al. (1983) and by Yano and Minato (1992).

The influence of moisture content on damping at room temperature has been reported by Suzuki (1980) and Sasaki et al. (1988). It was noted for hinoki (*Chamaecyparis obtusa*) that tan δ increased from 5.5 to 18.5×10^{-3} when moisture content increased from 5 to 35%. In the low temperature range (Fig. 4.31) for beech conditioned at various equilibrium moisture contents (4 or 27%) a phase transition, similar to those reported in other porous water-absorbing materials, was observed. Near the fiber saturation point, or more exactly at 27% moisture content, a phase transition of the same nature as "the glass transition of the absorbed water" was observed at −100 °C. Decreasing the moisture content of speci-

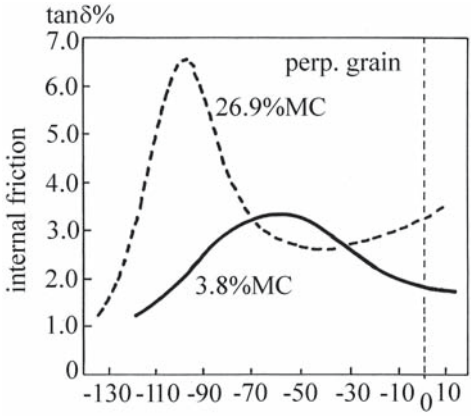

Fig. 4.31. Internal friction in the low temperature range for beech with different moisture content (*MC*). *perp. grain* Perpendicular to the grain. (Sellevold et al. 1975, with permission)

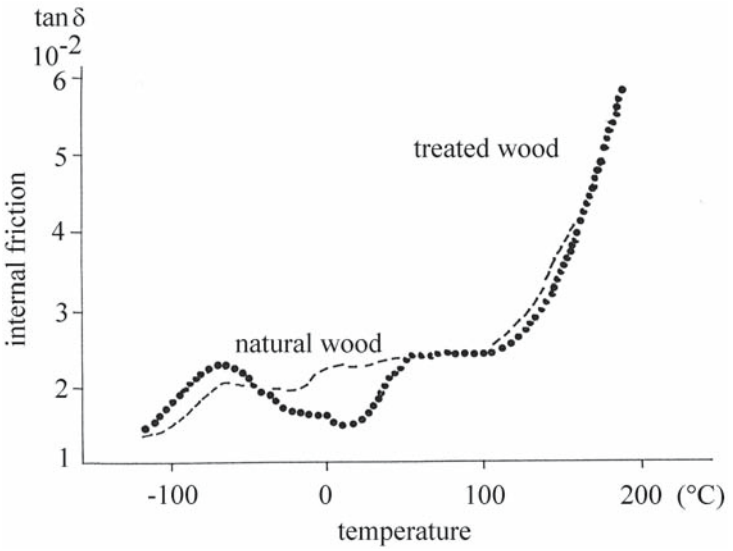

Fig. 4.32. Influence of zinc content on the dynamic behavior of wood ionomer – succinylated wood containing zinc compared with natural, untreated wood of *Tilia japonica*. (Nakano et al. 1990, with permission)

mens at 4% shifted the peak of internal friction to −60 °C, probably because of the presence of water mainly in the cell walls.

4.5.2.2 Chemical Treatment

The influence of chemical modification of the wood structure of *Tilia japonica* induced by a half-esterified treatment with zinc to obtain a succinylated wood ionomer can be observed by measuring tan δ in a wide temperature range (−120 to 230 °C) (Fig. 4.32). Two peaks are observed on this graph – at 180 and at −60 °C – probably corresponding to the restricted motion of the main cellulosic chain

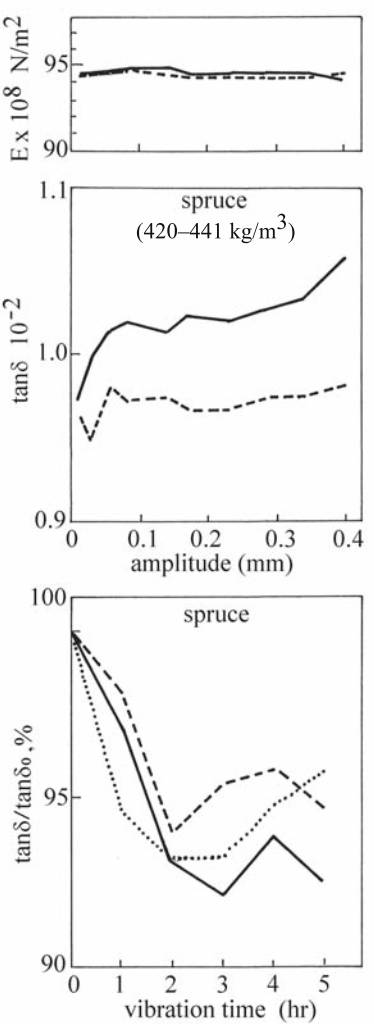

Fig. 4.33. Variation in the modulus of elasticity (*E*), internal friction, and ratios of internal friction versus the amplitude and vibration time of continuous flexural vibration of small amplitude [0.40 mm (*solid line*), 0.17 mm (*dashed line*), 0.03 mm (*dotted line*)] in spruce, measured in specimens of 35×5×400 mm, at frequency between 100 and 170 Hz. (Sobue and Okayasu 1992, with permission)

and to the side-chain motion, respectively (Nakano et al. 1990). In the region between −60 and 20 °C, corresponding to the micro-Brownian motion of half-esterified cellulose in the amorphous region and to the local vibration of carboxyl groups related to water molecules, tan δ decreased dramatically. At 20 °C its value is at a minimum. The increase in tan δ as the temperature rises to 60 °C indicates an increase in internal friction. Zn ions form intermolecular crosslinks between cellulose chains, and this structural modification of solid wood was also observed in tan δ measurements. The presence of metallic ions in the wood ionomer retards the thermal degradation of this material above 100 °C, as can be seen from the plateau of the graph in Fig. 4.32.

4.5.2.3 Dynamic Loading

Sobue and Okayasu (1992) showed that internal friction parameters measured in wood could be used for the estimation of very fine modifications of cellular wall structure induced by continuous vibration of specimens even with relatively small amplitudes. In Fig. 4.33, we observe that the value of E_L is not affected by the amplitude of 5 h of bending vibration, although the ratio $\tan \delta / \tan \delta_0$ ($\tan \delta_0$ corresponding to the initial state) decreased at a rate dependent on the vibration time and amplitude (i.e., 8% for 3 h at 0.40 mm amplitude). These results have been related to the chemical hydrogen bonds between the chains connecting the microfibrils and the lignin, and have been explained through the rate theory. Detailed calculations using the rate theory in wood can also be seen in Mark (1967) and Cousins (1974).

The results reported by Sobue and Okayasu (1992) can be brought together with the earlier experiments by Murphy (1963) using static tests at low stress levels. He found that the crystallinity of wood, measured by X-ray diffraction, increases with the rate of applied load. This behavior was related to the moderate-strength hydrogen bonds. Murphy proposed that when the matrix of the material is squeezed under stress, the connections were readjusted to give new bond positions. The intensity of the stress then produced either an elastic or a plastic response of the specimen.

Kohara et al. (1999) studied the relationship between the internal friction under a pulsated load and the acoustic emission behavior of spruce. The acoustic emission activity started at the limit of the linear viscoelastic region and the amplitudes of events were proportional to the internal friction. The damage procedure that induced acoustic emission is closely related to that of internal friction.

4.6 Summary

This chapter has highlighted the use of acoustical methods – vibrational in the audible range and ultrasonic – for characterization of the mechanical behavior of solid wood and wood-based composites. The following aspects have been discussed:

- The elastic symmetry of isotropic and anisotropic solids. The origin of the anisotropy, perceived as the variation of material response with direction of applied stress, lies in the preferred organization of the internal structure of the material (the orientation of "fibers " in solid wood or of layers in laminated wood-based composites). The terms of the independent elastic constants are presented: for example, 21 independent constants for monoclinic symmetry, nine constants for orthotropic symmetry, five for transverse isotropic material, and two for isotropic solids. The relationships between the technical engineering constants and the terms of stiffness and compliance matrices are discussed.
- The theoretical considerations related to wave propagation in anisotropic solids (Christoffel's equations), mainly in orthotropic solids, are presented because of the interest of the Cartesian orthotropic model for wood structure. Ultrasonic wave propagation phenomena in wood are illustrated in tridimensional representation of slowness surfaces and corresponding displacements. This representation underlines the kinematics of wave propagation related to

the progressive mode conversion and expresses better in a global way the differences between wood species in their acoustical behavior.

- The common audiofrequency acoustic methods for wood testing use frequencies below 20,000 Hz. Steady-state or transient (impact) excitation can be used for the dynamic tests at resonance vibration when elastic moduli are to be determined. The direct, accurate measurement of engineering constants of wood (three Young's moduli, three shear moduli, and six Poisson's ratios) is important in engineering and in product design. The most convenient technique for measuring these parameters with high precision depends upon measurements of the resonance frequencies of longitudinal, flexural, or torsional resonant modes of bar-shaped samples or plates. The technique can be extended to measure the internal friction if the quality factor Q or the logarithmic decrement are measured in addition to the resonance frequency.
- Specific aspects related to the measurement of the velocities of ultrasonic waves in wood are discussed. Wood material that is to be sensed and probed with ultrasonic waves might be divided into three main groups: trees and logs, small clear specimens, and engineering products. The practical success of ultrasonic methods is determined by the utilization of the appropriate transducers. The basic requirements of an ultrasonic transducer are: good sensitivity and resolution, controlled beam pattern, reproducible performance under various testing conditions, and high signal to noise ratio.
- The basis of the ultrasonic evaluation of the viscoelastic behavior of wood is associated with measurements of attenuation coefficients. The numerical significance of attenuation depends on the specific measurement conditions. Three main factors affecting the attenuation measurements in wood are the geometry of the radiation field (the geometry of the specimen) and the material characteristics of scattering and absorption (dependent on species, anisotropic direction, frequency, scale of observation, etc.). In the audible frequency range the viscoelastic behavior of wood is associated with the magnitude of the damping coefficients – the mechanical damping defined as “logarithmic decrement” or “tan δ” – for free vibrations and the quality factor Q for steady-state forced vibrations. The damping coefficients are indicators of microstructural modifications induced by temperature and moisture content, chemical treatment, mechanical loading of specimens, etc.